Draft version March 29, 2018
Typeset using LaTeX **preprint2** style in AASTeX61

NEW Y AND T DWARFS FROM WISE IDENTIFIED BY METHANE IMAGING*†

C. G. Tinney,[1,2] J. Davy Kirkpatrick,[3] Jacqueline K. Faherty,[4] Gregory N. Mace,[5] Mike Cushing,[6] Christopher R. Gelino,[3] Adam J. Burgasser,[7] Scott S. Sheppard,[8] and Edward L. Wright[9]

[1] *Exoplanetary Science at UNSW, School of Physics, UNSW Sydney, NSW 2052, Australia.*
[2] *Australian Centre for Astrobiology, UNSW Sydney, NSW 2052, Australia*
[3] *IPAC, Mail Code 100-22, Caltech, Pasadena, CA 91125*
[4] *Department of Astrophysics, American Museum of Natural History, New York, NY 10023*
[5] *McDonald Observatory and Department of Astronomy, University of Texas at Austin, Austin, TX 78712-1205, USA*
[6] *Department of Physics and Astronomy, The University of Toledo, OH 43606, USA*
[7] *Center for Astrophysics and Space Science, University of California San Diego, La Jolla, CA 92093*
[8] *Department of Terrestrial Magnetism, Carnegie Institution for Science, Washington, DC 20015, USA*
[9] *Department of Physics and Astronomy, UCLA, Los Angeles, CA 90095-1547, USA*

(Received 29 December 2017; Revised 21 February 2018; Accepted 27 March 2018)

Submitted to The Astrophysical Journal Supplement

ABSTRACT

We identify new Y- and T-type brown dwarfs from the *WISE All Sky* data release using images obtained in filters that divide the traditional near-infrared H and J bands into two halves – specifically CH_4s & CH_4l in the H and J2 & J3 in the J. This proves to be very effective at identifying cool brown dwarfs via the detection of their methane absorption, as well as providing preliminary classification using methane colours and *WISE* -to-near-infrared colours. New and updated calibrations between T/Y spectral types and CH_4s–CH_4l J3–W2, and CH_4s–W2 colours are derived, producing classification estimates good to a few spectral sub-types. We present photometry for a large sample of T and Y dwarfs in these filters, together with spectroscopy for 23 new ultra-cool dwarfs – two Y dwarfs and twenty one T dwarfs. We identify a further 8 new cool brown dwarfs, which we have high confidence are T dwarfs based on their methane photometry. We find that, for objects observed on a 4m-class telescope at J band magnitudes of $\sim$20 or brighter, CH_4s–CH_4l is the more powerful colour for detecting objects and then estimating spectral types. Due to the lower sky background in the J-band, the J3 and J2 bands are more useful for identifying fainter cool dwarfs at J$\gtrsim$22. The J3–J2 colour is poor at estimating spectral types. But fortunately, once J3–J2 confirms that an object *is* a cool dwarf, the J3–W2 colour is very effective at estimating approximate spectral types.

Keywords: Brown dwarfs; Techniques: photometric; Methods: observational
Corresponding author: C. G. Tinney
c.tinney@unsw.edu.au

* This paper includes data gathered with the 3.9m Anglo-Australian Telescope located at Siding Spring Observatory, Coonabarabran, Australia.

† This paper includes data gathered with the 6.5 meter Magellan Telescopes located at Las Campanas Observatory, Chile.

1. INTRODUCTION

Data from the NASA Wide-field Infrared Survey Explorer (WISE; Wright et al. 2010; Mainzer et al. 2011) have delivered unprecedented advances in our understanding of the properties and space densities of the coldest compact astrophysical sources identified outside our Solar System – the T- and Y-type brown dwarfs(e.g., Cushing et al. 2011; Kirkpatrick et al. 2011, 2012; Kirkpatrick et al. 2013). These very cold brown dwarfs have scientific impacts that span multiple astronomical arenas. In the field of star formation, they can deliver a historical record of the star formation process at very low masses and at epochs billions of years prior to the star forming regions we observe today. In the field of planetary atmospheric theory, they represent low-temperature atmospheres that can be readily observed without the contaminating glare of a host star, and without the photochemical complications introduced by host star irradiation. In the field of exoplanet searches, they provide nearby, low-luminosity search targets potentially hosting planetary systems of their own, which would have implications for the debate on what differentiates a low-mass brown dwarf from a high-mass planet.

WISE readily identifies these very cold brown dwarfs as a result of their strong thermal infrared methane absorption. The shortest wavelength *WISE* band (hereafter W1) has a central wavelength of 3.4 μm, which sits in the middle of the strong fundamental methane absorption band near 3.3 μm. The second shortest *WISE* band (hereafter W2), has a central wavelength of 4.6 μm, where the photosphere is reasonably transparent and so detects flux from deeper, hotter layers in the brown dwarf. As a result, cold brown dwarfs can be identified via their very red W1–W2 colour. WISE's relatively uniform all-sky coverage, coupled with its ability to identify cool objects even when quite close to the Galactic plane, makes it the ideal data source from which to generate a complete thermal-infrared magnitude-limited sample of T and Y dwarfs in the Solar Neighbourhood. The generation of just such a T/Y-dwarf census is a key goal of the *WISE Science Team* brown dwarf collaboration. Large numbers of Y- and T-type brown dwarfs have been identified and spectroscopically confirmed to date by the *WISE Science Team* brown dwarf collaboration using both colour selection (see e.g., Mainzer et al. 2011; Cushing et al. 2011; Kirkpatrick et al. 2011, 2012; Tinney et al. 2012; Mace et al. 2013), and more recently supplemented by proper-motion selection from the *AllWISE* and *NEOWISE* samples (see e.g., Kirkpatrick et al. 2014; Schneider et al. 2016a; Kirkpatrick et al. 2016). Additional cool brown dwarfs have been found by multiple teams independently working with public *WISE* data (e.g., Pinfield et al. 2014; Luhman 2014), while others have been identified from searches for cool companions to nearby stars companions to nearby stars (e.g., Luhman et al. 2011; Liu et al. 2012; Dupuy et al. 2015).

The *WISE Science Team* brown dwarf collaboration has largely selected targets for follow-up on the basis of photometry consistent with W1−W2 > 2.9 over the full range of *WISE* W2 magnitudes, plus somewhat bluer objects (i.e. down to W1−W2 = 2.0) if colours and magnitudes suggested a distance less than 20 pc. In many cases these objects are non-detections at W1 (i.e. their W1−W2 colours are 3-σ upper limits). This substantially increases the observational phase space probed by this follow-up program, at the cost of increasing the number of "false positives" identified from the *WISE* data, which must then be eliminated by subsequent observations.

Follow-up observations require the identification and spectral classification of a near-infrared counterpart to the *WISE* source. Unfortunately, the coldest objects (i.e. the Y dwarfs) can be *very* faint in the near-infrared (i.e. $J \sim H \gtrsim 22$), making them challenging targets even for 8 m-class ground-based telescopes. T dwarfs in *WISE* will be somewhat brighter in the near-infrared, and this gives medium-sized 4 m-class telescopes a role in targeting them as part of the completion of the *WISE* T/Y-dwarf census.

Methane imaging can play a useful role in this process. The discovery of very strong and broad methane absorption in the spectrum of the known T dwarf (Gl 229B Nakajima et al. 1996; Oppenheimer et al. 1996) made the use of this spectral signature for T-dwarf identification using specially designed imaging filters self-evidently obvious. This was confirmed when Rosenthal et al. (1996) use a circularly variable filter (i.e. an adjustable narrow band filter) to differentially re-detect Gl 229B. Subsequent use of methane imaging (rather than spectroscopy) to "winnow" out T dwarfs from wide-field survey data was first carried out by Herbst et al. (1999), while the first use of methane filters in blind searches for new T dwarfs was carried out by Mainzer & McLean (2003). At around the same time Tinney et al. (2005) began using specially constructed methane filters in the IRIS2 instrument at the Anglo-Australian Telescope to identify T dwarfs from lists of candidates from the 2MASS survey.

The power of this technique for *WISE* follow-up comes from the fact that the identification of a near-infrared counterpart that shows methane absorption within a small distance on the sky from a *WISE All-Sky* or *AllWISE* position uniquely identifies this near-infrared object as the counterpart to the *WISE* source. Following which, the strength of the methane absorption can then provide a spectral type estimate, reducing the necessity for spectroscopic follow-up in all cases.

2. IMAGING – ANGLO-AUSTRALIAN TELESCOPE (AAT)

Imaging observations were carried out on the AAT on the nights listed (as local dates) in Table 1 with IRIS2 (Tinney et al. 2005). IRIS2 is a near-infrared imager and spectrograph, with a single 1024×1024 pixel detector giving an imaging field of view of 7.7′ on a side at a pixel scale of 0.4486″/pixel.

Data were obtained in seeing conditions ranging from 1.05″ to over 2.0″. Targets for observation were selected in 2011 from then extant catalogues using the pipeline software developed to produce the *WISE* Preliminary Data Release (for details see the Explanatory Supplement[1]), and in 2012 from the *WISE All-Sky* release. As the optimal candidate selection procedures were being developed at the same time as improved versions of the *WISE* pipeline, we report in Table 2 the *WISE* photometry for our observed sources as presented in the *WISE* All-Sky data release made in March 2012 (rather than the photometry based on which they were originally selected).

In general the selected candidates satisfy the criteria that they were detected in W2 and had W1–W2>2.0. The *WISE* processing pipeline records either detections at greater than 3-σ significance, or 3-σ upper limits. Requiring a W1 detection (or 3-σ upper limit) and W1–W2>2.0, pushes the effective W2 detection floor much brighter than that imposed by the pipeline's 3-σ detection threshold. Our faintest T and Y dwarf candidates typically had W2 $\lesssim$ 15.5, which corresponds to a signal-to-noise ratio of

[1] http://wise2.ipac.caltech.edu/docs/release/prelim/expsup/

Table 1. AAT CH_4s,CH_4l Methane Imaging.

Run	Prog.	Useful Nights	Seeing
2011 Jun 11-18	11A/14	...	...
2011 Sep 6-13	11B/26	Sep 6,7,10,12,13	1.05-1.5″
2012 May 30-Jun 3	12A/27	May 30,31	1.2-2.0″
2012 Jun 27-30	12A/27	Jun 28,29,30	1.2-2.0″
2012 Sep 4-6	12B/26	Sep 4,5,6	1.4-2.2″
2012 Dec 28-Jan 1	12B/26	Dec 28,29,30,31,Jan 1	1.2-2.6″

∼10. Additional selection criteria have been found to greatly assist in improving the rejection of non-brown dwarf contaminants. Broadly we require the source was not identified as an artifact (i.e., known to be spurious), and that it wasn't flagged as blended (in which case it would have poorly determined photometry). For more details, including values of the specific flags used, see §2.1 of Kirkpatrick et al. (2012).

2.1. *J-band imaging*

Each candidate was initially observed in J-band with a planned exposure time of 54 minutes, broken up into thirty-six 90s pseudo-randomly dithered exposures. On-line data reduction using the ORACDR pipeline system (Cavanagh et al. 2008)[2] would then produce a near-publication-quality processed sub-mosaic soon after the first 9 images of this dither pattern were completed. This processed image was then analysed using purpose-built Perl scripts that automated the extraction of photometry for the image (using SExtractor; Bertin & Arnouts 1996), followed by the photometric and astrometric calibration of that data using the 2MASS Point Source Catalog (PSC; Skrutskie et al. 2006).

[2] See also http://www.oracdr.org/

This meant that within 5 minutes of the completion of the first 9-image sub-mosaic, we would know whether a J-band positional counterpart had been identified down to J≈19.5. If a positionally matched candidate clearly emerged after this first sub-mosaic (when such an object emerged they usually did so at the >10-σ level), then the dithering sequence would be truncated, and methane imaging observations begun. In the absence of an "early" match the J-band imaging sequence was allowed to run to completion, providing imaging data to a depth of J≈21.

2.2. *Methane imaging*

Once a plausible J-band counterpart had been identified, methane imaging observations were carried out with the CH_4s and CH_4l filters in IRIS2. The use of these filters for the study of cool brown dwarfs is described in Tinney et al. (2005) – we summarise just the salient points here. The IRIS2 methane filters (CH_4s and CH_4l) divide the H-band in half, sampling the wavelength ranges 1.520-1.620 μm and 1.640-1.740 μm (respectively). Flux in the CH_4l filter is substantially depressed by methane absorption in T and Y dwarfs, and so the CH_4s–CH_4l colour provides a powerful means of determining T and Y dwarf classifications. Methane filter observations are obtained by interleaving CH_4s and CH_4l observations (in an ABBA sense), while also dithering the telescope on sky. These data are also processed "on the fly" by ORACDR and deliver pairs of reduced images after every 7-9 pairs of images, which are then processed and differentially calibrated onto the CH_4s–CH_4l photometric system of Tinney et al. (2005). As with the J-band imaging, purpose-built scripts are run as soon as the first pair of CH_4s and CH_4l mosaics are produced. Once again, if a clear methane signature was detected the observing sequence was truncated, and observations moved on to the next *WISE*

candidate.

2.3. *Photometry*

Following the initial processing done at the telescope, the ORACDR pipeline was used to reprocess these data for final analysis. A simple two-step process is followed: in the first step *all* images on each object are processed together to produce a flat-field and a first-pass mosaic, allowing the flattened images that went into this first-pass mosaic to be analysed to determine their photometric zero-point and image quality; in the second-pass, frames with poor image quality or poor photometric throughput are culled and the remaining images reprocessed to produce a final mosaic. Photometry was then obtained from the final mosaics on each field, by differentially calibrating onto the J_{MKO} or CH_4s–CH_4l systems using 2MASS PSC photometry for stars lying within the IRIS2 field of view.

For J band data this differential calibration is achieved by identifying objects in the field of view with 2MASS $-0.2 < J - K < 1.5$ and the converting those J magnitudes from the 2MASS photometric system to the MKO photometric system, using the equations determined by J. Carpenter in the 2MASS All-sky Survey Explanatory Supplement[3]. As the IRIS2 J,H,K,Ks filters are MKO ones (i.e. manufactured to the prescriptions of Tokunaga et al. 2002), the result is J photometry on the MKO system.

For CH_4s,CH_4l data, objects in the field-of-view for which transformations from the 2MASS to MKO photometric systems are reliable (i.e. have 2MASS colours in ranges where the Carpenter transformations are valid – see Tinney et al. 2005) are converted to MKO H, and then used to define zero-points for the CH_4s and CH_4l systems, and so determine CH_4s–CH_4l. The resulting zero-points for a given field are typically determined to between ±0.02-0.1 mag, and the scatter about the zero-point determination is used to determine a standard error in the mean, which is then propagated to the finally quoted photometric uncertainties.

Table 2 presents J and CH_4s–CH_4l photometry from the AAT, as well as *WISE* W1 and W2 photometry from the *All-Sky* release – the official *WISE* designation for all sources combines the prefix "WISE" with the position designation in column 1 of the table – e.g. WISE J001505.87-461517.6. These are abbreviated thereafter with the letter "W" and the first four digits of the right ascension and declination of the designation – e.g. W0015-4615. Also listed in the table are spectral types resulting from spectroscopic observations in this paper (§5) and other programs, as well as estimated spectral types based on a new CH_4s–CH_4l calibration derived in §6.1.

[3] http://www.ipac.caltech.edu/2mass/releases/allsky/doc/sec6_4b.html

Table 2. *WISE* , J_{MKO} and CH_4s–CH_4lphotometry for candidate cool *WISE* brown dwarfs

WISE Desig.[a]	W1	W2	W1−W2	J_{MKO}[b]	CH_4s[c]	CH_4s–CH_4l[c]	CH_4 SpT[d]	J−W2	CH_4s−W2	Spec	Notes
T/Y dwarfs : Position matches with unresolved sources showing CH_4 absorption.											
J001505.87−461517.6	17.02 0.15	14.25 0.06	2.77 0.16	17.76 0.06	17.45 0.06	−1.24 0.16	T7.0 0.5	3.51 0.09	3.23 0.08	T8	FIRE, this paper
J003231.09−494651.4	18.08 0.34	15.07 0.09	3.01 0.35	18.54 0.09	18.20 0.07	−1.96 0.23	T8.6 0.5	3.47 0.13	3.13 0.11	T8.5	FIRE, this paper
J014807.25−720258.7	>18.94	14.69 0.05	>4.25	···	18.77 0.05	−2.34 0.20	T9.2 0.5	···	4.08 0.07	T9.5	Kirkpatrick et al. 2012
J024124.73−365328.0	16.89 0.10	14.34 0.04	2.55 0.11	16.59 0.04	16.55 0.03	−1.06 0.06	T6.5 0.5	2.25 0.06	2.21 0.08	T7	FIRE, this paper
J030919.67−501614.3	16.51 0.08	13.61 0.03	2.90 0.09	17.17 0.03	17.01 0.03	−1.31 0.06	T7.2 0.5	3.56 0.10	3.40 0.05	···	
J032504.33−504400.3	>18.73	15.70 0.10	>3.03	18.94 0.09	18.39 0.09	−2.20 0.36	T9.0 0.5	3.24 0.13	2.69 0.13	T9	Schneider et al. 2015
J035000.32−565830.2	>18.90	14.73 0.06	>4.17	22.47 0.49	···	···	···	7.74 0.51	···	Y1	Kirkpatrick et al . 2012
J040443.48−642029.9	>18.86	15.73 0.09	>2.60	19.55 0.22	19.43 0.04	−1.27 0.10	T7.1 0.5	3.82 0.23	3.70 0.10	T9	Schneider et al. 2015
J041022.71+150248.4	>18.33	14.18 0.06	>4.15	···	20.47 0.07	···	···	···	6.29 0.09	Y0	Kirkpatrick et al. 2012
J062842.71−805725.0	>18.78	15.45 0.08	>3.32	18.71 0.16	18.34 0.04	−2.30 0.13	T9.1 0.5	3.26 0.18	2.89 0.09	···	
J064528.38−030248.2	>18.18	14.94 0.10	>3.24	16.91 0.04	16.88 0.04	−1.00 0.09	T6.3 0.5	1.97 0.12	1.94 0.15	T6	SpeX, this paper
J071322.55−291751.9	>18.35	14.48 0.06	>3.87	19.64 0.15	19.33 0.04	−2.72 0.15	T9.7 0.5	5.16 0.16	4.85 0.08	Y0	Kirkpatrick et al. 2012
J071301.84−585445.1	>19.04	15.44 0.07	>3.60	···	···	···	···	···	···	T9	FIRE, this paper
J072227.27−054029.9[e]	15.19 0.05	12.21 0.03	2.98 0.06	16.52 0.02	16.39 0.02	−2.12 0.04	T8.9 0.5	4.31 0.03	4.18 0.03	T9[f]	Kirkpatrick et al. 2012
J091408.96−345941.5	>17.83	15.03 0.09	>2.80	18.36 0.11	17.79 0.02	−1.70 0.07	T8.2 0.5	3.33 0.14	2.76 0.10	T8	FIRE, this paper
J094020.10−220820.5	17.01 0.14	14.57 0.07	2.43 0.16	17.36 0.05	17.30 0.04	−1.52 0.11	T7.8 0.5	2.79 0.17	2.73 0.08	T8	SpeX, this paper
J105553.59−165216.3	>18.37	15.04 0.10	>3.33	20.79 0.02	20.35 0.06	< −1.69	>T8.2	5.75 0.11	5.31 0.14	T9	FIRE, this paper
J111239.24−385700.7	17.97 0.40	14.36 0.06	3.61 0.40	20.26 0.15	19.94 0.05	−1.72 0.12	T8.2 0.5	5.90 0.16	5.58 0.08	T9	FIRE, this paper
J114156.71−332635.8	17.20 0.17	14.53 0.06	2.67 0.18	19.76 0.14	19.69 0.04	(−0.71 0.09)[g]	(T5.4 0.5)[g]	5.23 0.15	5.16 0.07	Y0	FIRE, this paper
J143311.42−083736.4	>18.74	15.23 0.10	>3.51	19.07 0.11	···	···	···	3.84 0.15	···	T8[h]	FIRE, this paper
J144806.48−253420.3	>18.28	15.03 0.09	>3.25	18.85 0.11	18.71 0.13	−1.02 0.29	T6.4 0.5	3.82 0.14	3.68 0.16	T8	FIRE, this paper
J150115.92−400418.4	16.48 0.11	14.21 0.05	2.07 0.12	16.53 0.04	16.05 0.03	−0.86 0.06	T5.9 0.5	2.32 0.06	1.84 0.05	T6	SpeX, this paper
J173551.72−820900.1	15.61 0.06	13.73 0.04	1.88 0.07	16.58 0.03	16.41 0.03	−0.76 0.08	T5.6 0.5	2.85 0.05	2.68 0.05	T6	FIRE, this paper
J201748.72−342102.5	>18.21	15.09 0.13	>3.12	20.89 0.24	20.19 0.06	−1.46 0.15	T7.7 0.5	5.80 0.27	5.10 0.14	···	
J205628.91+145953.2	>18.25	13.93 0.05	>4.33	···	18.99 0.04	−3.17 0.25	Y0.2 0.5	···	5.06 0.06	Y0	Kirkpatrick et al . 2011
J210200.15−442919.5	16.94 0.17	14.12 0.05	2.83 0.18	18.25 0.06	18.06 0.06	−2.20 0.24	T9.0 0.5	4.13 0.08	3.94 0.08	T9	NIRSPEC, this paper
J215949.48−480854.9	17.76 0.29	14.54 0.07	3.19 0.30	18.89 0.08	18.64 0.09	−1.31 0.28	T7.2 0.5	4.35 0.11	4.10 0.13	T9	FIRE, this paper
J221140.52−475826.5	17.67 0.21	14.58 0.06	3.09 0.22	17.38 0.04	17.38 0.04	−1.51 0.14	T7.8 0.5	2.80 0.07	2.80 0.07	···	

Table 2 continued

Table 2 *(continued)*

WISE Desig.[a]	W1	W2	W1−W2	J_{MKO}[b]	CH_4s[c]	CH_4s–CH_4l[c]	CH_4 SpT[d]	J−W2	CH_4s−W2	Spec	Notes
J221216.33−693121.6	18.05 0.40	14.90 0.09	3.15 0.41	19.72 0.13	19.29 0.04	−3.15 0.23	Y0.2 0.5	4.82 0.16	4.39 0.10	T9.5	FIRE, this paper
J222055.31−362817.4	>18.65	14.66 0.06	>3.99	20.38 0.17	20.20 0.07	< −1.52	>T7.8	5.72 0.18	5.58 0.09	Y0	Kirkpatrick et al . 2012
J223204.50−573010.5	>17.90	15.15 0.11	>2.75	18.86 0.09	18.74 0.10	−1.49 0.30	T7.7 0.5	3.71 0.14	3.59 0.14	T9	FIRE, this paper
J230228.68−713441.6	17.14 0.14	14.28 0.05	2.86 0.14	16.97 0.04	17.52 0.07	−1.14 0.15	T4.7 0.5	2.69 0.06	3.24 0.09	···	
J233226.49−432510.6	>17.88	14.99 0.09	>2.89	···	19.14 0.04	< −2.59	>T9.5	···	4.15 0.09	T9:	NIRSPEC, this paper
J235425.33−564928.6	16.93 0.13	14.84 0.08	2.09 0.15	17.09 0.04	16.98 0.04	−0.55 0.07	T7.8 0.5	2.25 0.09	2.14 0.09	T6	FIRE, this paper
J235447.80−814044.9	18.23 0.33	15.03 0.07	>3.20	17.64 0.05	17.68 0.06	−1.04 0.12	T6.4 0.5	2.61 0.09	2.65 0.10	···	
T/Y dwarfs : Position matches (<1″) with an extended source, sources showing no methane absorption and/or non-detections.											
J012102.92−190656.9	16.47 0.09	14.71 0.07	1.76 0.11	19.67 0.16	18.87 0.13	+0.17 0.17	···	4.96 0.17	4.16 0.15	···	i
J071939.54−173514.8	16.72 0.07	13.71 0.03	3.01 0.08	···	20.1 0.1	+0.33 0.15	···	···	6.39 0.17	···	j
J074551.79−015122.1	18.14 0.41	14.97 0.09	3.17 0.42	19.90 0.16	19.53 0.15	+0.25 0.20	···	4.93 0.17	4.56 0.17	···	i
J083942.85−402938.9	17.37 0.24	13.66 0.04	3.71 0.25	20.6 0.2	18.82 0.11	+0.40 0.15	···	6.94 0.22	5.16 0.12	···	k
J130740.45−463035.1	15.00 0.03	12.93 0.03	2.07 0.04	···	16.59 0.04	+0.24 0.05	···	···	3.66 0.05	···	l
J150711.06−344026.0	15.64 0.06	14.03 0.05	1.62 0.08	17.73 0.04	17.18 0.05	+0.26 0.07	···	3.70 0.07	3.15 0.09	···	m
J164445.19−645628.9	>18.50	15.22 0.10	>3.28	···	18.13 0.09	+0.15 0.11	···	···	2.91 0.13	···	i
J185709.40−315345.5	16.48 0.12	14.42 0.07	2.06 0.14	18.58 0.10	17.84 0.09	+0.05 0.12	···	4.16 0.12	3.42 0.11	···	i
J190230.27−371246.1	17.18 0.21	14.46 0.07	2.72 0.22	20.27 0.29	···	···	···	5.81 0.30	···	···	n
J193441.70−490837.6	17.00 0.12	14.50 0.06	2.50 0.13	20.36 0.31	···	···	···	5.86 0.32	···	···	See Table 4
J203020.25−692043.0	18.06 0.43	14.83 0.09	3.23 0.44	19.51 0.17	18.83 0.15	-0.07 0.23	···	4.68 0.20	4.00 0.17	···	o
J203119.30−690500.3	>17.58	14.41 0.07	>3.17	20.44 0.22	19.18 0.03	-0.41 0.06	T4.2 0.5	6.03 0.23	4.77 0.08	···	p
J224245.85−201511.0	>18.32	15.15 0.13	>3.17	20.03 0.16	···	···	···	4.88 0.21	···	···	q

Table 2 continued

Table 2 *(continued)*

WISE Desig.[a]	W1	W2	W1−W2	J_{MKO}[b]	CH_4s[c]	CH_4s–CH_4l[c]	CH_4 SpT[d]	J−W2	CH_4s−W2	Spec	Notes

[a] *WISE* object designations and photometry are from the March 2012 release of the All-sky Source Catalog, unless an "A" prefix is used in which case they come from the November 2013 AllWISE Source Catalog release. The All-Sky WISE designation combines the prefix "WISE" with the position designation (i.e. WISE J001505.87-461517.6 for an All-sky Source and WISEA J030237.53−581740 for an AllWISE Source). These are abbreviated with the first four digits of the right ascension and declination throughout this paper – e.g. W0015-4615.

[b] IRIS2 J photometry was obtained through a J_{MKO} filter, differentially calibrated using J_{2MASS} photometry converted to J_{MKO} in each field.

[c] IRIS2 CH_4sand CH_4s–CH_4lphotometry calibrated (as described in the text) on the system of Tinney et al. (2005).

[d] Estimated spectral types using CH_4s–CH_4l and the calibration of §6.1.

[e] The discovery name for this object is UGPS J072227.51-054031.2 (Lucas et al. 2010) and J_{MKO} is from that paper.

[f] While noting that the spectral type for this object has been the subject of some debate, we adopt the T9 type of Kirkpatrick et al. (2012)

[g] The methane colour of W1141 suggests a spectral type of ≈T5.5, however the J–W2 colour is indicative of a type of T9 or later. As discussed in the text and shown in Fig. 2, the CH_4s–CH_4l (and especially the CH_4l) photometry is contaminated by a background galaxy.The J3−W2 photometry (§6.3) and the FIRE spectrum (§5) clearly show this to be a Y0. We do not include this object in the CH_4s–CH_4l calibration of §6.1.

[h] 143311.42−083736.4: A spectrum and spectral type for this object has also been published by Lodieu et al. (2012). Those values are in agreement with those presented here.

[i] J012102.92-190656.9, J074551.79-015122.1, J164445.19-645628.9 and J185709.40-315345.5: a bright source has a position match with the *WISE* position. The CH_4s-CH_4l colours indicates they are not T dwarfs.

[j] J071939.54-173514.8: extended source at position with no methane absorption

[k] J083942.85-402938.9: is clearly an extended source (2.1″×3.0″), with no methane absorption. WISE source is likely this galaxy.

[l] J130740.45-463035.1: a bright CH_4s=16.60 source has a position match with the *WISE* position, and shows no proper motion since the 2MASS epoch.. The CH_4s-CH_4l colour indicates this object is not a T dwarf.

[m] J150711.06-344026.0: this bright W2 source was observed as a poor conditions backup target and it has a position match with the *WISE* position, but the CH_4s-CH_4l colour indicates this object is not a T dwarf. Shows no proper motion since the 2MASS epoch).

[n] J190230.27-371246.1: very extended (3.5″) source at position, making this galaxy the likely WISE source.

[o] J203020.23-692043.1: has excellent position match object with J=19.51, however this is marginally resolved (2.2″ fwhm) in 2.0″ seeing, and shows no methane absorption. It is likely the *WISE* flux arises from this galaxy.

[p] J203119.30-690500.3 has excellent position match object with J=20.44 and methane absorption. However the object is resolved at J (2.2″ fwhm in 2.0″) and H (1.84″ fwhm in 1.39″ seeing). Moreover, the methane colour suggests a spectral type of T4 which is inconsistent with the J-W2 and CH_4s-W2 colours (which suggest a much later spectral type of >T9). This identification is therefore considered tentative.

[q] J224245.85-201511.0 has J=20.03 object 1.2″ from the *WISE* position. However, this object has an almost identical J and J2 magnitudes which suggests methane absorption would be extremely weak.

Table 3. Magellan J2/J3 Methane Imaging.

UT Date	Median Seeing (″)
2012 Mar 10	0.64
2012 May 10	0.56
2012 Jul 6	0.70
2012 Jul 7	0.53
2013 Jan 15	0.40
2013 Mar 22	0.56
2013 Apr 22	0.57
2013 Aug 15	0.50
2016 Nov 18	0.80
2017 Jan 05	0.54

3. IMAGING – MAGELLAN

Imaging observations were obtained using the FourStar imaging camera (Persson et al. 2013) on the Magellan Baade telescope between March 10, 2012 and January 5, 2017. FourStar is a near-infrared mosaic imager with four 2048×2048 pixel detectors giving an imaging field of view of 11′ on a side at a pixel scale of 0.159″/pixel. It is equipped with a set of intermediate-band filters, originally specified for the measurement of photometric redshifts. These filters turn out to be almost ideally suited for observing very cool brown dwarfs (see Fig.1 in Tinney et al. 2012). In particular, the J3 filter ($\lambda_{cen} \approx 1.29\,\mu$m, 90% of peak throughput range 1.210-1.366 μm) collects almost all of the "methane free" J-band flux from late-T and Y dwarfs, while the J2 filter ($\lambda_{cen} \approx 1.14\,\mu$m, 90% of peak throughput range 1.067-1.224 μm) is strongly impacted by methane absorption between 1.1 μm and 1.2 μm. All the observations described here were performed with the *WISE* target positioned in FourStar's Chip 2.

Image quality over the course of this program varied between 0.4″ and 0.7″ (see Table 3). Our observing and analysis techniques follow those previously described by us (Tinney et al. 2012, 2014), and involve observing each target with the FourStar J3 and J2 filters in a sequence of 60-120s pseudo-randomly dithered exposures. Targets are observed with net integration times ranging from 5 minutes to 1.0h. As with the AAT data, images are processed at the telescope using a modified version of the ORACDR[4] data reduction pipeline, and examined during observing to determine whether a counterpart had been detected. As for the AAT data, the final analysis involves running ORACDR twice for each jitter set, with individual exposures of poor image quality removed from the list used in the second-pass.

Photometric processing and calibration followed the procedures outlined above for AAT data, except for the final stage of calibration onto the J2/J3 photometric system, which followed that outlined in Tinney et al. (2012). That is, 2MASS sources in the field-of-view were calibrated onto the J_{MKO} system, and we used this MKO photometry for stars in the range $0.4 < (J–K)_{MKO} < 0.8$ to define the zero-point for the J2 and J3 magnitude system. Table 4 presents J2 and J3 photometry from Magellan, as well as *WISE* W1 and W2 photometry (as contained in the March 2012 *WISE All-Sky* data release).

[4] http://www.jach.hawaii.edu/JACpublic/UKIRT/software/oracdr

Table 4. *WISE* and Magellan J3,J2 photometry of candidate cool brown dwarfs from *WISE*

WISE Designation[a]	W1	W2	W1−W2	J3[b]	J3-J2	J3−W2	Est. SpT[c]	SpT	Notes
T/Y dwarfs : Position matches with unresolved sources showing CH_4 absorption.									
AJ004206.84−584023.9	18.86 0.49	15.60 0.10	3.26 0.50	17.76 0.04	−1.10 0.06	2.16 0.11	T6.6	···	
J014807.25−720258.7	>18.94	14.69 0.05	>4.25	18.83 0.02 (9)[d]	−1.72 0.12	4.16 0.07	T8.9	T9.5	Kirkpatrick et al. 2013
AJ030237.53−581740.3	>19.26	15.81 0.09	>3.45	20.76 0.11	−1.52 0.27	4.95 0.14	T9.5	Y0	FIRE, this paper
J064723.23−623235.5	>19.09	15.32 0.08		22.51 0.09 (2)	−1.21 0.20	7.19 0.12	Y0.9	Y1	Kirkpatrick et al. 2014
J071322.55−291751.9	>18.35	14.48 0.06	>3.87	19.42 0.03 (8)	−1.58 0.06	4.94 0.0	T9.5	Y0	Kirkpatrick et al. 2012
J081117.81−805141.3	17.29 0.12	14.38 0.04	2.91 0.13	19.31 0.01 (6)	−1.71 0.09	4.95 0.04	T9.5	T9.5	Mace et al. 2013
J091408.96−345941.5	>17.83	15.03 0.09	>2.80	17.73 0.02	−1.29 0.03	2.70 0.09	T7.4	T8	FIRE, this paper
AJ102313.22−315126.7	>18.94	15.76 0.12	>3.18	18.24 0.03	−1.12 0.06	2.48 0.13	T7.1	T8	FIRE, this paper
J111239.24−385700.7	17.97 0.40	14.36 0.06	3.61 0.40	20.11 0.04 (4)	−1.36 0.11	5.77 0.07	Y0.1	T9	FIRE, this paper
J114156.71−332635.8	17.20 0.17	14.53 0.06	2.67 0.18	19.63 0.05 (6)	−1.30 0.10	5.22 0.08	T9.7	Y0	FIRE, this paper
J122152.28−313600.8	15.86 0.06	13.85 0.04	2.01 0.07	15.80 0.03	−1.14 0.05	1.95 0.05	T6.3	T5.5	Mace et al. 2013
J150115.92−400418.4	16.48 0.11	14.21 0.05	2.07 0.12	15.95 0.01	−1.06 0.02	1.74 0.05	T5.8	T6	SpeX, this paper
J163940.83−684738.6	>17.89	13.65 0.05	>4.24	20.62 0.08	−1.65 0.12	6.98 0.09	Y0.8	Y0	Tinney et al. 2012
AJ172907.10−753017.0	18.74 0.38	15.55 0.08	3.19 0.39	17.71 0.02	−1.09 0.04	2.16 0.08	T6.6	T7	FIRE, this paper
J173551.72−820900.1	15.61 0.06	13.73 0.04	1.88 0.07	16.17 0.01	−1.09 0.01	2.44 0.05	T6.9	T6	FIRE, this paper
AJ204928.59−443143.9	>18.94	15.64 0.11	>3.30	18.22 0.03	−1.39 0.06	2.58 0.11	T7.3	···	
J210200.15−442919.5	16.94 0.17	14.12 0.05	2.83 0.18	18.08 0.01 (11)	−1.52 0.14	3.96 0.06	T8.7	T9	NIRSPEC, this paper
J233226.49−432510.6	>17.88	14.99 0.09	>2.89	19.13 0.02 (6)	−1.64 0.18	4.19 0.10	T8.9	T9:	NIRSPEC, this paper
T/Y dwarfs : Position matches (<1″) with an extended source, sources showing no methane absorption and/or non-detections.									
J080811.36−682521.2	>19.27	16.18 0.11	>3.08	20.97 0.07	+0.12 0.09				e
J083440.09−643616.4	>18.79	14.75 0.05	>4.04	20.29 0.03	-0.21 0.05				f
J092958.73−712733.0	>19.29	16.40 0.14	>2.89	···	···	···	···	···	g
J093730.46−735454.0	>18.97	16.15 0.12	>2.81	19.47 0.05	-0.29 0.07				h
J101242.66−482842.3	>18.66	15.73 0.12	>2.93	20.86 0.06	-0.26 0.10				i
J102719.82−443656.7	18.12 0.47	15.20 0.09	2.92 0.47	20.48 0.04	-0.38 0.07				j
J103059.32−373140.3	>18.25	15.78 0.17	>2.48	20.41 0.08	-0.13 0.11				k
J120906.70−520034.5	>18.82	15.85 0.13	>2.97	21.44 0.10	-0.07 0.13				l
J122329.62−480051.3	>18.51	15.85 0.16	>2.66	20.78 0.08	-0.07 0.11				m

Table 4 continued

Table 4 *(continued)*

WISE Designation[a]	W1	W2	W1−W2	J3[b]	J3-J2	J3−W2	Est. SpT[c]	SpT	Notes
J123252.86−800525.4	>18.47	15.88 0.15	>2.59	...	...	...	...	...	n
J124156.18−370345.5	17.78 0.22	14.87 0.06	2.91 0.23	20.49 0.03	-0.11 0.05				o
J130348.35−460959.4	>18.79	16.09 0.18	>2.71	21.60 0.06	+0.08 0.08				p
J143032.81−323321.7	17.11 0.17	14.72 0.08	2.39 0.19	20.57 0.04	-0.49 0.07				q
J153802.79−450936.5	>17.96	14.90 0.10	>3.06	See note					r
J171507.17−552116.8	>17.23	14.60 0.08	>2.63	20.74 0.05	-0.21 0.08				s
J193441.70−490837.6	17.00 0.12	14.50 0.06	2.50 0.13	20.50 0.05	-0.12 0.08				t
J211213.88−552855.5	>18.55	15.83 0.18	>2.71	21.46 0.08	-0.36 0.13	...	...	...	u
J212505.20−323412.9	>18.48	15.06 0.11	>3.42	20.21 0.03	-0.11 0.05				v
J220011.60−544914.2	>17.37	14.86 0.11	>2.51	19.78 0.03	-0.11 0.04				w
J221342.90−294908.7	17.87 0.43	14.59 0.09	3.28 0.44	20.73 0.01	-0.14 0.04				x
Unconfirmed methane absorbers within 30″ of *WISE* position									
J011020.86−132313.0	>18.247	14.85 0.18	>3.39	...	...	...	...	...	aa
J092320.42−731704.1	>19.124	16.68 0.19	>2.45	...	...	...	...	...	bb
AJ183437.34−584119.4	>18.714	15.67 0.11	>3.04	...	...	...	...	...	cc

Table 4 continued

Table 4 *(continued)*

WISE Designation[a]	W1	W2	W1−W2	J3[b]	J3-J2	J3−W2	Est. SpT[c]	SpT	Notes

[a] *WISE* designations follow Table 2

[b] FourStar J3 and J2 photometry processed as described in Tinney et al. (2014, 2012). J3 observations with numbers in parentheses are the average of the indicated number of independent observations, and the uncertainty is the standard error in the mean. For other observations the uncertainty is the photon-counting and calibration zero-point uncertainties combined in quadrature.

[c] Estimated spectral type from J3−W2 colour and the calibration described in §6.3.

[d] The J3 photometry reported here corrects the incorrect value in Table 1 of Tinney et al. (2012).

[e] J080811.36−682521.2: Object 0.5″ from *WISE* position with no methane absorption. No methane absorbers within 30″ to J3=22

[f] J083440.09−643616.4: Galaxy (resolved in 0.48″ seeing) 0.2″ from *WISE* . No methane absorbers within 30″ to J3=22.

[g] J092958.73−712733.0: No objects with methane absorption within 30″ to J3=21

[h] J093730.46−735454.0: Object 0.5″ from *WISE* position with no methane absorption. No methane absorbers within 30″ to J3=21.5

[i] J101242.66−482842.3: Object 0.6″ from *WISE* position with no methane absorption. No methane absorbers within 30″ to J3=22

[j] J102719.82−443656.7: Unresolved object (in 0.5″ seeing) with no methane absorption 0.2″ from *WISE* , plus J3=21.0 galaxy 1.7″" from WISE position. This pair would be confused in WISE & likely cause of W1–W2 colour. No methane absorbers within 30″ to J3=22

[k] J103059.32−373140.3: Object with no methane absorption 1.9″ from *WISE* position. No methane absorbers within 30″ to J3=21

[l] J120906.70−520034.5: Object with no methane absorption 0.5″ from *WISE* position. No methane absorbers within 30″ to J3=21

[m] J122329.62−480051.3: Object with no methane absorption 1.5″ from *WISE* position. No methane absorbers within 30″ to J3=21.5

[n] J123252.86−800525.4: No sources within 10" of WISE position to J=21. No methane absorbers within 30″.

[o] J124156.18−370345.5: Galaxy (resolved in 0.48″ seeing) 0.3″from *WISE* position. No methane absorbers within 30″ to J3=22.5

[p] J130348.35−460959.4: Galaxy (1.0×0.8″ in 0.55″ seeing) at WISE position. No methane absorbers within 30″ to J3=22.5

[q] J143032.81−323321.7: Galaxy (resolved in 0.47″ seeing) 0.3" from *WISE* position. No methane absorbers within 30″ to J3=22

[r] J153802.79−450936.5: Crowded field with multiple objects (J3=19.3, 20.4,17.1,21.4,21.5,21.0) within 5″ of *WISE* position, none with methane absorption. No methane absorbers within 30″ to J3=21.5

[s] J171507.17−552116.8: Unresolved source (0.6″ seeing) with no methane 0.5″ from *WISE* . No methane absorbers within 30″ to J3=22.5

[t] J193441.70−490837.6: J3=20.5 galaxy (1.1″ resolved in 0.9″ seeing) 0.2″ from *WISE* . No methane absorbers within 30″ to J3=21.5

[u] J211213.88−552855.5: Object 2.4″ from *WISE* position with no methane absorption. No methane absorbers within 30″ to J3=21.5

[v] J212505.20−323412.9: Galaxy 0.7″from *WISE* position. One methane absorber 21″ from *WISE* at 21:25:06.3 -32:33:56 with J3=21.3, J3−J2=−0.84±0.12, but galaxy is the more likely *WISE* source.

[w] J220011.60−544914.2: Galaxy (1.0″ resolved in 0.6″ seeing) 0.4″ from *WISE* position. No methane absorbers within 30″ to J3=22

[x] J221342.90−294908.7: Galaxy (0.7×0.6″) 0.3″ from WISE position with no methane. No methane absorbers within 30″ to J3=22

[aa] J011020.86−132313.0: Only candidate methane absorber is J3=21.0, J3−J2=−0.88±0.08, but 32.6″away from *WISE* position at 01:10:18.7 −13:2322 requires ∼ 11″/yr motion to be the *WISE* source. If a match would have J3−W2=6.17 suggesting a possibly Y0.

[bb] J092320.42−731704.1: Only candidate methane absorber within 30″ is J3=21.1, J3−J2=−0.96±0.18, 19.4″ from *WISE* position at 09:23:20.4 −73:16:44. If a match would would require a ∼3″/yr motion, and J3−W2=4.42 would suggest a T9-T9.5.

[cc] J183437.34−584119.4: Only candidate methane absorber within 30″ is J3=22.4, J3−J2=−1.2±0.2, 14.0″ from *WISE* position at 18:34:36.5 -58:41:06. If a match would would require a ∼3″/yr motion, and J3−W2=6.8±0.2 which would suggest a Y0.

4. IMAGING SUMMARY

The *WISE* candidates observed naturally fall into a few classes:

(a) a bright (i.e. $J < 19.5$) object is readily detected as a positional match with the *WISE* source. In 100% of cases, these objects are subsequently confirmed by methane imaging as T dwarfs;

(b) a fainter (i.e. $19.5 < J < 21.5$) object is detected as a positional match that (in some cases) we have been able to verify is a T- or Y-dwarf using either methane imaging, or spectroscopy obtained on other telescopes in parallel with this methane imaging program);

(c) either a fainter (i.e. $19.5 < J < 21.5$) object is detected as a positional match with photometry that is inconsistent with this object being a T/Y dwarf, *or* we observe the object to be resolved in good imaging at Magellan indicating the *WISE* source is most likely a galaxy; or

(d) no counterpart is detected down to J∼21.5-22 – these could either be contaminant sources (i.e. non-cool-brown-dwarfs whose *WISE* photometry mimics those of brown dwarfs due to confusion, photometric scatter, etc) or cool brown dwarfs fainter than $J \sim 22$.

Finding charts for objects newly identified as being a T- or Y-dwarfs are provided in Fig. 1. Figure 2 shows expanded images at the position of the new Y0 dwarf W1141-3326. These show how the 2012 CH_4s–CH_4l photometry for this object was contaminated by confusion with a background source. The images from 2014 (by which time W1141-2236 had moved ≈2″ to the west) show W1141-2236 clearly separated from this background source. It is also clear that in the 2012 images, CH_4s is more contaminated that CH_4l making CH_4s–CH_4l more positive than it should be. We therefore exclude W1141-3336 from our updated CH_4s–CH_4l-to-spectral-type calibration in §6.1.

4.1. *Brown dwarf proper motions*

Figure 1 highlights the complicating factor of proper motion when seeking to identify cool brown dwarfs. The charts for W2049-4431, W2159-4808, W1112-3857 and W1141-3326 (for example) all show substantial motion between the epoch of the *WISE* detection (mean *WISE* epochs are in the range 2010 Apr-Jun for these four targets) and the epoch of follow-up (from 2011 Sep to 2017 Jan).

The observed motions of our new WISE T and Y dwarfs are summarised in Table 5. We obtained astrometry for our J, CH_4s, or J3 images by cross-matching against the 2MASS PSC and relying on *WISE* and the PSC being on the same co-ordinate system. The individual positional uncertainty of the *WISE* objects (0.3-0.5″) is the dominant source of uncertainty, so this is a good assumption. Note that we distinguish between the "apparent" motion of our targets from just two epochs as observed by *WISE* and our IRIS2 or FourStar follow-up imaging (here denoted μ'), and the true proper motion from an astrometric solution that includes parallax. The large *WISE* position uncertainties mean that the uncertainty in the right ascension and declination components of μ' are very similar, so only a single uncertainty is quoted for both in the Table. This uncertainty includes an additional term added in quadrature of 100 mas to account for possible parallax motion not being accounted for in objects that could be as close as 10 pc away. Five of these brown dwarfs are the subject of our on-going astrometric program with FourStar, so we provide preliminary proper motion solutions (in this case including a parallax solution) for comparison. In each case the solutions agree, although the FourStar

astrometric solutions are between 10 and 20 times better than the *WISE* –IRIS2/FourStar estimates.

Motions of $0.5''\,\mathrm{yr}^{-1}$ are not uncommon, and the motions observed for the most rapidly moving brown dwarfs (W0032-4946 $\sim$1.5″ yr^{-1}, W2159-4808 $\sim$1.4″ yr^{-1}, W1141-3326 $\sim$0.95″ yr^{-1}, W1112-3857 $\sim$0.9″ yr^{-1}, W2049-4431 $\sim$0.7″ yr^{-1}) highlight how identification via "blind" spectroscopy becomes substantially more difficult after just a few years. After 5 years the positional error box that must be searched can be as large as 20″ on a side, and can contain multiple objects that would have to be spectroscopically observed in turn to find the correct T/Y-dwarf. In this situation methane imaging becomes an even more powerful tool to pick out the correct counterpart.

5. OBSERVATIONS – SPECTROSCOPY

Follow-up spectroscopy is the "gold standard" for confirming a T- or Y-dwarf identification. Spectroscopic observations have therefore been carried out by members of the *WISE* Science Team brown dwarf collaboration on a variety of telescopes in parallel with our imaging program at the AAT and Magellan. We report here spectroscopy obtained on multiple nights between 2011 Sep 8 and 2017 Jan 05 (Table 6).

5.1. *Magellan/FIRE*

The Folded-port Infrared Echellette (FIRE; Simcoe et al. 2008, 2010) at the 6.5m Walter Baade Telescope on Cerro Manqui at the Las Campanas Observatory, Chile, uses a 2048×2048 HAWAII-2RG array. In prism mode, it covers a wavelength range from 0.8 to 2.5 μm at a resolution ranging from R=500 at J-band to R=300 at K-band for a slit width of 0.6″. FIRE was used to obtain spectroscopy of T dwarf candidates on the nights listed in

Table 5. Apparent (μ') and Proper (μ) Motions for new cool brown dwarfs from *WISE*

Object[a]	*WISE* –IRIS2/FouStar			FourStar alone		
	μ'_α	μ'_δ	Unc.	μ_α	μ_δ	Unc.
	(mas yr^{-1})			(mas yr^{-1})		
W0015−4615	+720	−450	±250			
W0032−4946	−714	−1300	±250			
W0042−5840	+122	−140	±120			
W0241−3653	+350	+100	±230			
W0302−5817	−86	−150	±120			
W0309−5016	+645	+100	±270			
W0404−6420	−139	+180	±155			
W0628−8057	+110	−550	±150			
W0645−0302	−43	−430	±160			
W0914−3459	−160	−20	±180			
W0940−2208	−70	+30	±160			
W1023−3151	−220	+250	±110			
W1055−1652	−728	+250	±160			
W1112−3857	+510	+590	±180	+666	+638	±10
W1141−3326	−915	+120	±180	−897	−84	±6
W1221−3136	+550	+360	±180			
W1433−0837	−130	0	±240			
W1448−2534	+110	−670	±180			
W1501−4004	+580	−290	±170			
W1729−7530	+30	−230	±120			
W1735−8209	−350	−540	±230			
W2017−3421	+385	+10	±240			
W2049−4431	+415	−585	±120			
W2102−4429	−250	−340	±240	+41	−354	±3
W2159−4808	+275	−1380	±240			
W2211−4758	−170	−160	±240			
W2212−6931	+600	+200	±240			
W2220−3628	+320	+60	±250	+283	−94	±4
W2232−5730	+240	+80	±170			
W2302−7134	−220	0	±160			
W2332−4325	+200	−315	±250	+248	−256	±4
W2354−5649	+390	−330	±160			
W2354−8140	+30	−15	±230			

[a] *WISE* designations follow Table 2

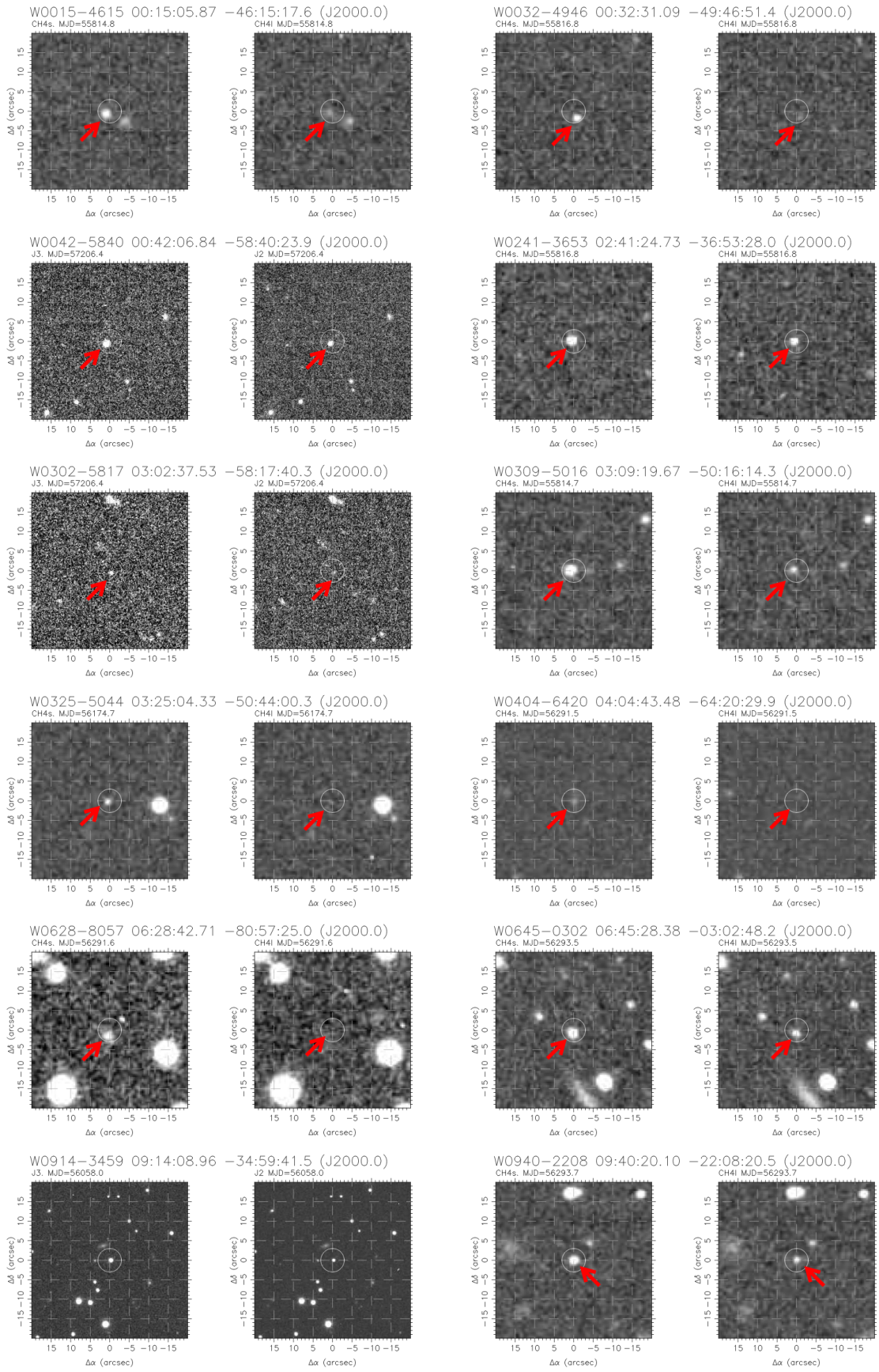

Figure 1. Pairs of finding charts in CH_4s/CH_4l or J3/J2 for the imaging observations tabulated in Tables 2 and 4. All charts are 40″ on a side, N top the top, W to the right, centred on the *WISE* source position and with a 3″ circle drawn at the *WISE* position. Methane absorbing objects are brighter in the left panel of each pair of images. In ambiguous cases, an arrow is used to identify the cool brown dwarf.

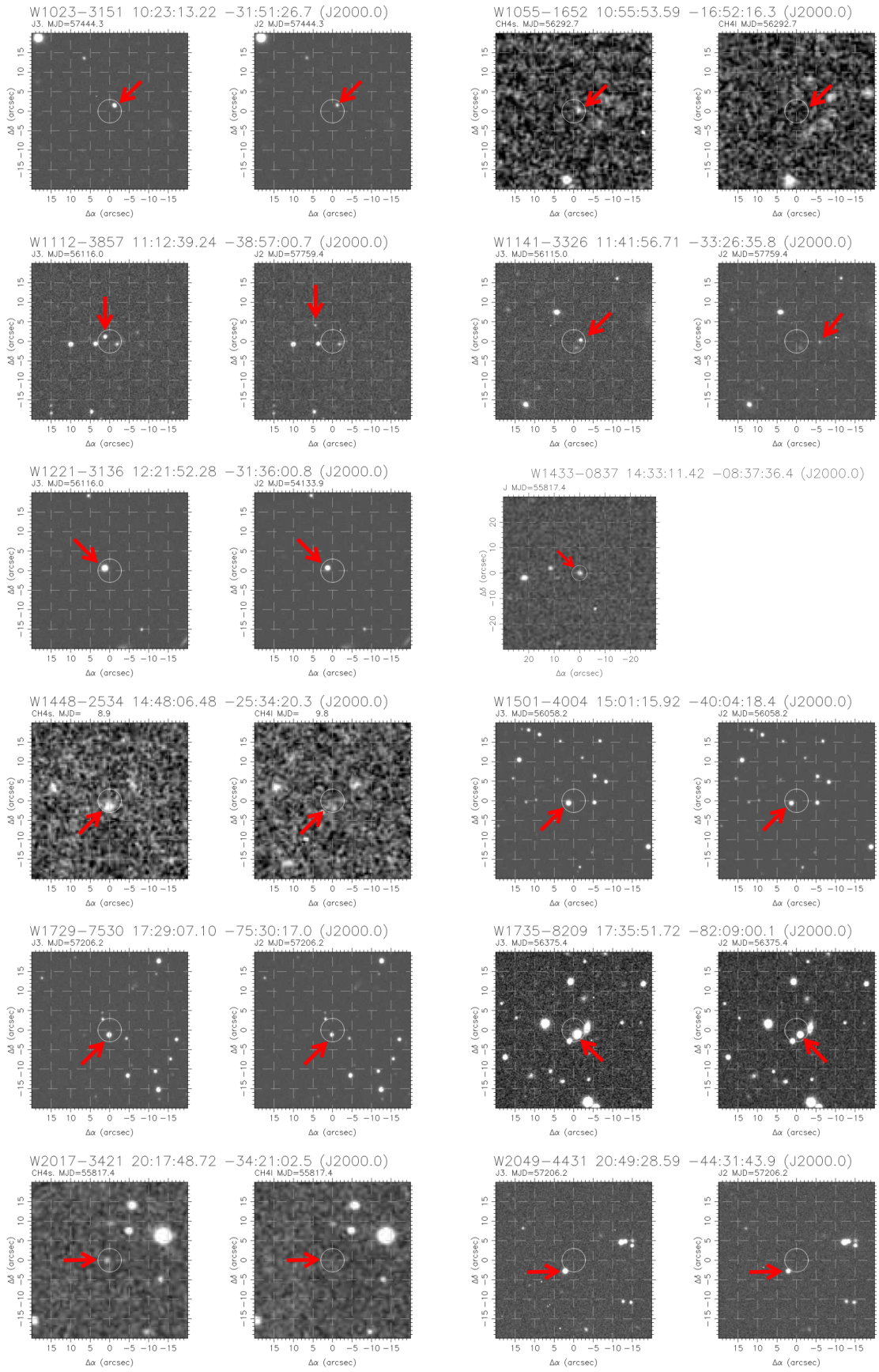

Figure 1 (cont). The single image of W1433-0837 is a J band one from the AAT, with the arrow indicating the object observed spectroscopically.)

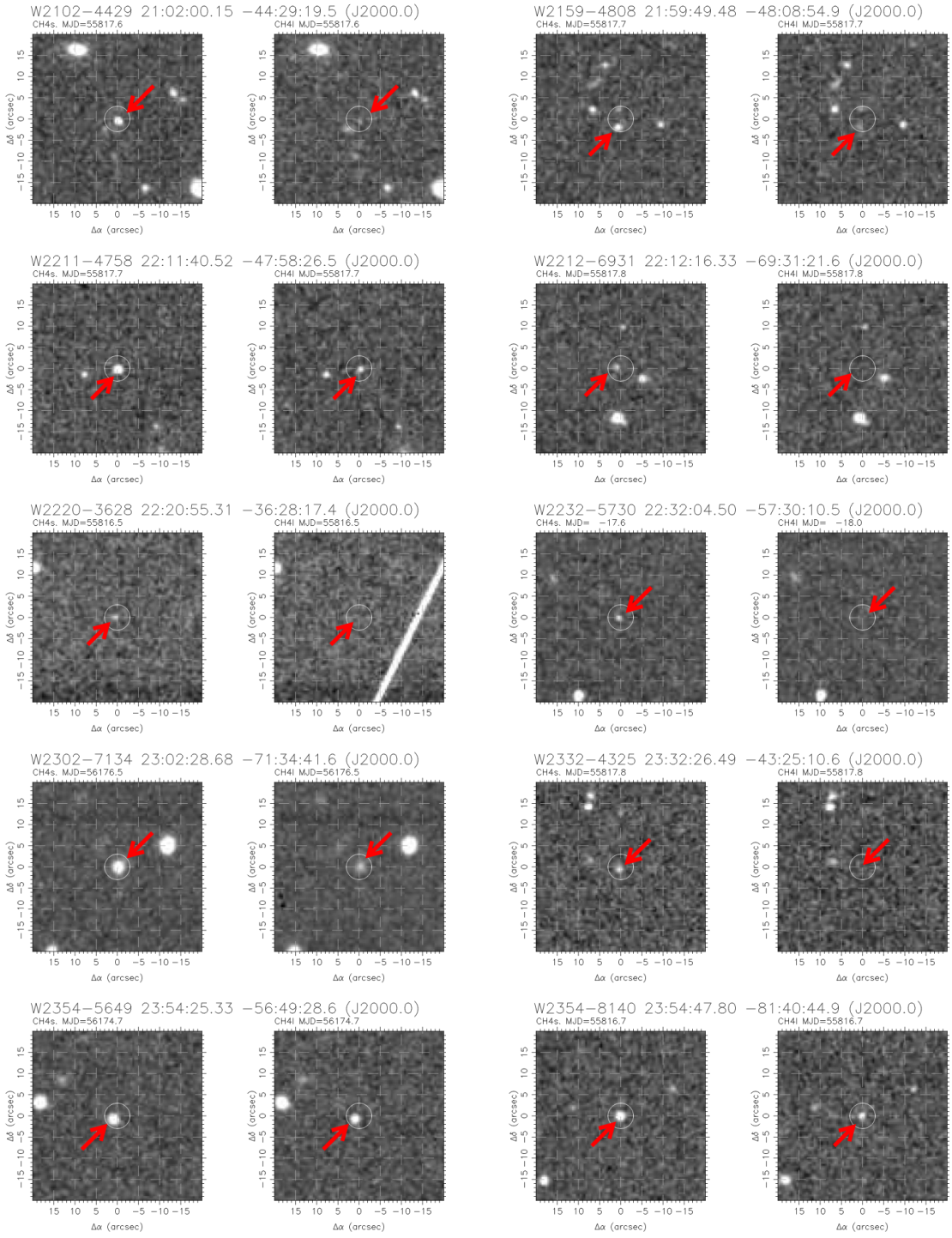

Figure 1 (cont).

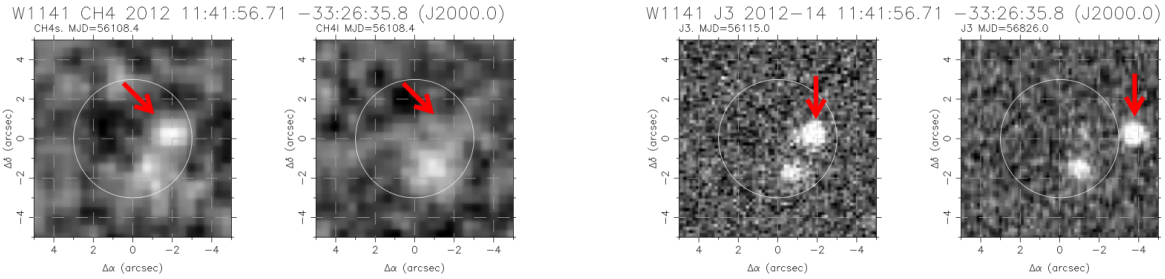

Figure 2. Zoomed images 10″ on a side at the location of W1141-3326. CH_4s and CH_4l images from 2012 are shown on the left, and J3 images from 2012 and 2014 are shown on the right. W1141-3326's proper motion moved it 2″ to the W between July 2012 and June 2014, and away from a group of background sources that clearly contaminated the CH_4l photometry in 2012, producing a spuriously red CH_4s–CH_4l colour.

Table 6. WISE Cool Dwarf Spectroscopy

WISE Designation	UT Date	Telescaope	Exp. (s)	Sp. Type
J001505.87−461517.6	2012 Jan 05	Magellan[b]	1014	T8
J003231.09−494651.4	2012 Jan 05	Magellan[b]	1268	T8.5
J024124.73−365328.0	2011 Sep 08	Keck[d]	600	T7
AJ030237.53−581740.3	2017 Jan 05	Magellan[c]	2700	Y0:
J064528.38−030248.2	2013 Mar 04	IRTF	2400	T6
J071301.84−585445.1	2012 May 06	Magellan[b]	1200	T9
J091408.96−345941.5	2016 Mar 23	Magellan[c]	900	T8
J094020.10−220820.5	2013 Mar 04	IRTF	1600	T8
AJ102313.22−315126.7	2016 Mar 23	Magellan[c]	900	T8
J105553.59−165216.3	2013 Mar 22	Magellan[c]	800	T9:
J111239.24−385700.7	2012 May 06	Magellan[b]	1680	T9
J114156.71−332635.8	2014 Mar 10	Magellan[c]	2000	Y0
J143311.42−083736.4	2012 Jan 17	Magellan[b]	240	T8
J144806.48−253420.3	2014 Mar 10	Magellan[c]	800	T8
J150115.92−400418.4	2014 Mar 04	IRTF	2000	T6
AJ172907.10−753017.0	2016 Mar 23	Magellan[c]	900	T7
J173551.72−820900.1	2016 Mar 23	Magellan[c]	600	T6
J210200.15−442919.5	2011 Oct 09	Keck[d]	4200	T9
J215949.48−480854.9	2012 May 05	Magellan[b]	1400	T9
J221216.33−693121.6	2012 May 06	Magellan[b]	1400	T9.5
J223204.50−573010.5	2012 May 06	Magellan[b]	1400	T9
J233226.49−432510.6	2011 Oct 09	Keck[d]	4200	T9:
J235425.33−564928.6	2016 Nov 18	Magellan[c]	1200	T6

[a] *WISE* designations follow Table 2

[b] Data processing carried out with FIREHOSE package as described in the text.

[c] Data processing carried out with Figaro package as described in the text.

[d] These are the same spectra used to obtain spectral types by Kirkpatrick et al. (2012), albeit independently classified in this paper (Fig. 3). In both cases we obtain the same types as Kirkpatrick et al.

Table 6. FIRE reductions in this paper were carried out in two ways. Roughly half the spectra were processed in the same manner as the spectroscopy presented in Tinney et al. (2012) using the Figaro data reduction package, with telluric removal carried out using A0 spectra acquired immediately before or after the science target at similar airmass. Remaining objects were processed using the FIREHOSE package for low-dispersion data following the procedure in the online "cookbook"[5]. For our faintest objects, pair subtraction prior to insertion into the pipeline greatly improved the accuracy of the sky-line fitting procedure. The combined spectrum was then corrected for telluric absorption and flux calibrated using observations of an A0 V star and the technique described in Vacca et al. (2003) and the XTELLCOR program from SpeXtool (see Cushing et al. 2004).

5.2. *Keck/NIRSPEC*

The Near-Infrared Spectrometer (NIRSPEC; McLean et al. 1998, 2000) at the 10m W. M. Keck Observatory on Mauna Kea, Hawaii, was used to obtain confirmation spectroscopy of several new T dwarfs. For spectroscopy, NIRSPEC uses a 1024×1024 InSb array. The NIRSPEC observations employed the $42''\times0\farcs57$ slit, providing a resolution R∼1500. Our brown dwarf candidates were observed in the N3 configuration (see McLean et al. 2003) that covers part of the J-band window from 1.15 to 1.35 μm. Data reduction made use of the publicly available REDSPEC package, with modifications to remove residuals from the sky-subtracted pairs prior to 1-D spectral extraction.

5.3. *IRTF/SpeX*

SpeX is a medium-resolution spectrograph and imager at NASA's 3m Infrared Telescope Facility (IRTF) on Mauna Kea, Hawai'i. It uses a 1024×1024 InSb array for its spectroscopic observations (Rayner et al. 2003). We used the prism mode with a $0\farcs5$ wide slit to achieve a resolving power of $R \equiv \lambda/\Delta\lambda \approx 150$ over the range 0.8-2.5 μm. A series of 200s exposures were typically obtained at two different positions along the $15''$ long slit. A0 dwarf stars were observed soon after or before the target

[5] See http://www.mit.edu/people/rsimcoe/FIRE/ob_data.htm for details.

and at similar airmass, and used for telluric correction and flux calibration. A set of exposures of internal flat field and argon arc lamps were obtained for flat fielding and wavelength calibration.

The data were reduced using Spextool (Cushing et al. 2004) the IDL-based data reduction package for SpeX. The raw images were first corrected for non-linearity, pair subtracted, and then flat fielded. For some of the fainter sources, multiple pair-subtracted images were averaged in order to facilitate tracing. The spectra were then optimally extracted (e.g., Horne 1986) and wavelength calibrated using the argon lamp exposures. Multiple spectra were then averaged and the resulting spectrum was corrected for telluric absorption and flux calibrated using observations of an A0 V star using the technique described in Vacca et al. (2003).

5.4. *Spectral Types*

The objects listed in Table 6 were spectrally classified using the near-infrared T0-to-T8 dwarf sequence of Burgasser et al. (2006), extended to later T and Y dwarfs by Cushing et al. (2011) and Kirkpatrick et al. (2012). (See Table 7 for the specifically adopted standard spectra). Assignment of types was performed by overplotting these standards onto the candidate spectra and determining by-eye which standard provided the best match. In some cases two adjacent standards, such as T8 and T9, provided an equally good match, so the candidate spectrum was assigned an intermediate type (in this example, T8.5). In Figure 3 we show the near-infrared spectra for all of our sources compared with the relevant spectral standard. We consider these types to have an uncertainty of ±0.5 subtypes. Types which are more uncertain due to low signal-to-noise-ratio spectra (i.e. ±1 sub-type) are marked with a colon ":" next to the spectral type.

Table 7. Adopted Spectral Standards.

Spectral Type	Full Designation	Short Designation
T5	2MASS J15031961+2525196	2M1503
T6	SDSS J162414.37+002915.6	S1624
T7	2MASS J07271824+1710012	2M0727
T8	2MASS J04151954−0935066	2M0415
T9	UGPS J072227.51−054031.2	U0722
T9.5	WISE J014807.25−720258.7	W0148
Y0	WISEPA J173835.53+273258.9	W1738
Y0.5	WISEPA J154151.66−225025.2	W1541
Y1	WISE J035000.32−565830.2	W0350

6. DISCUSSION

6.1. *An Updated CH_4s–CH_4l Spectral Type Calibration*

Tinney et al. (2005) have presented a calibration between the IRIS2 CH_4s–CH_4l colour and spectral type. Cardoso et al. (2015) have used very similar filters on the NICS instrument on the Telescope Nazionale Galileo and derived a calibration using the same functional form as Tinney et al. (2005), but with slightly different values. With the additional methane imaging data for later-type objects available in Table 2 we have updated this calibration to derive the relation shown in the upper panel of Fig. 4. A relation with a simple functional form (like that used by Tinney et al.) proved to be impossible to obtain, and so we have instead used a spline calibration, which we present as the sequence shown in Table 8. The scatter about this calibration over the whole spectral type range is 0.11 mag. More importantly for the use of CH_4s–CH_4l colours to estimate spectral types, the slope of the relation for types beyond T5 is very steep, so that typical measurement errors of ±0.1 mags in the colour map

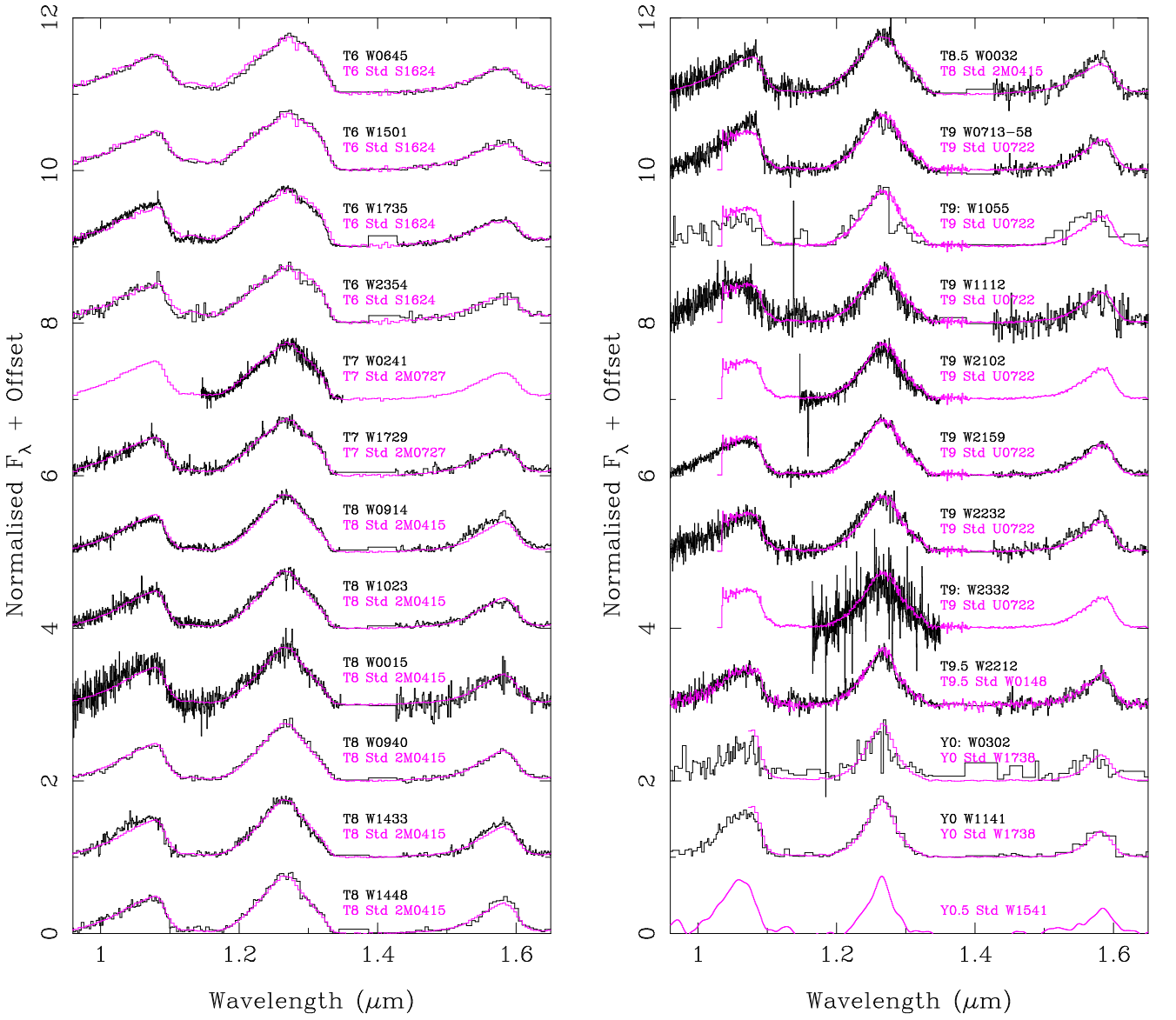

Figure 3. T and Y dwarf spectra listed in Table 6 plotted to demonstrate spectral classifications derived as described in the text. Each new spectrum *(black lines)* is over plotted with the relevant spectral standard *(magenta lines)*.

into uncertainties in spectral type estimates of less than ±0.3 sub-types for all objects later than T5. We therefore adopt an uncertainty for our estimated T and Y types in Table 2 of better than 0.5 sub-types.

The lower left panel of Fig. 4 shows an expanded version of this plot, along with the calibration relations due to Tinney et al. (2005) and Cardoso et al. (2015). The authors of the latter have already noted that their calibration is systematically redder (in CH_4s–CH_4l) for a given spectral type than the earlier calibration. Examination of their Fig. 4 suggests that this may be due to either a fortuitous observation of a sample of objects lying above the sequence of Tinney et al. (2005), or a systematic difference in the colour terms driven by the optics of NICS on the Telescopio Nazionale Galileo, or both. (The filters and detectors in both IRIS2

and NICS are identical, so the only the rest of the optical train can plausibly produce this difference.) The addition of further very late objects in our new sample of T and Y dwarfs brings our new calibration and that of Cardoso et al. (2015) into much closer alignment for all objects later than T7, while the differences at earlier types now seem consistent with cosmic scatter about the calibration.

The lower right panel of Fig. 4 plots the resulting estimated spectral types against actual spectral types, for objects from both this paper and Tinney et al. (2005). In the vast majority of cases the estimated spectral types predicted based on CH_4s-CH_4l colour are in line with the spectroscopic types – 70% of the objects plotted have estimated types agreeing with their observed types to within ±0.5 types, and 91% agree to within ±1 type. The most prominent exception is W1141-3326, which (as already noted) was found to be *much* later when a spectrum was acquired (Y0), than predicted (T5), due to confusion with a background object. Of the 5 objects observed to deviate by more than 1 whole spectral type from their predicted type, four are in the sense that the observed type was *later* than predicted. Indeed only one of 53 objects was found to be earlier than predicted by more than a whole spectral type, which reinforces the power of these filters for robustly and rapidly identifying (and approximately typing) T- and Y-type dwarfs – if imaging detects a methane absorption signature in an unresolved object (i.e. not a galaxy) near the position of a *WISE* or 2MASS candidate object, then it is almost certainly a legitimate match with the *WISE* or 2MASS candidate, making it a T or Y dwarf. If the estimated type that results is in "error" it is more likely to predict the object to be earlier, rather than later. (A similar result was found by Cardoso et al. 2015). These results give us confidence in the T dwarf identifications even for the eight T dwarfs in Tables 2 & 4 for which spectroscopy has not yet been obtained.

Table 8. CH_4s–CH_4l versus Spectral Type

SpT	CH_4s-CH_4l	SpT	CH_4s-CH_4l	SpT	CH_4s-CH_4l
A0	0.000	M4	0.132	T2	-0.035
A5	0.000	M6	0.150	T3	-0.157
F0	0.000	M8	0.169	T4	-0.350
F5	0.000	L0	0.185	T5	-0.595
G0	0.001	L2	0.199	T6	-0.900
G5	0.015	L4	0.198	T7	-1.250
K0	0.050	L6	0.178	T8	-1.600
K3	0.076	L8	0.123	T9	-2.200
M0	0.099	T0	0.080	Y0	-3.000
M2	0.115	T1	0.043	Y1	-4.000

6.2. *J3–J2 versus Spectral Type*

To observe fainter cool dwarfs (i.e. J$\gtrsim$21 candidates where methane observations in the H-band with CH_4s,CH_4l filters on the 4m AAT became problematic) we made use of methane sensitive filters in the J-band (i.e. the J3 and J2 filters installed in FourStar). These J-band filters see a substantially lower sky background than the equivalent H-band filters, while the blue colours of late T and Y dwarfs mean they see essentially the same flux as in the H-band. This combination makes it feasible to target fainter objects down to J$\sim$22-24 – and in one extreme case to J3$\sim$25 (Faherty et al. 2014).

We take this opportunity to note that the faintest ground-based near-infrared detection of a Y-dwarf (WISE J085510.83-071442.5 at J3=$24.8^{+0.5}_{-0.35}$) reported by Faherty et al. (2014) has been the subject of some debate (Schneider et al. 2016b; Luhman & Esplin 2016). The claimed discrepancy here is almost certainly not real, but rather a result of issues associated with conversion to a standard MKO J passband from

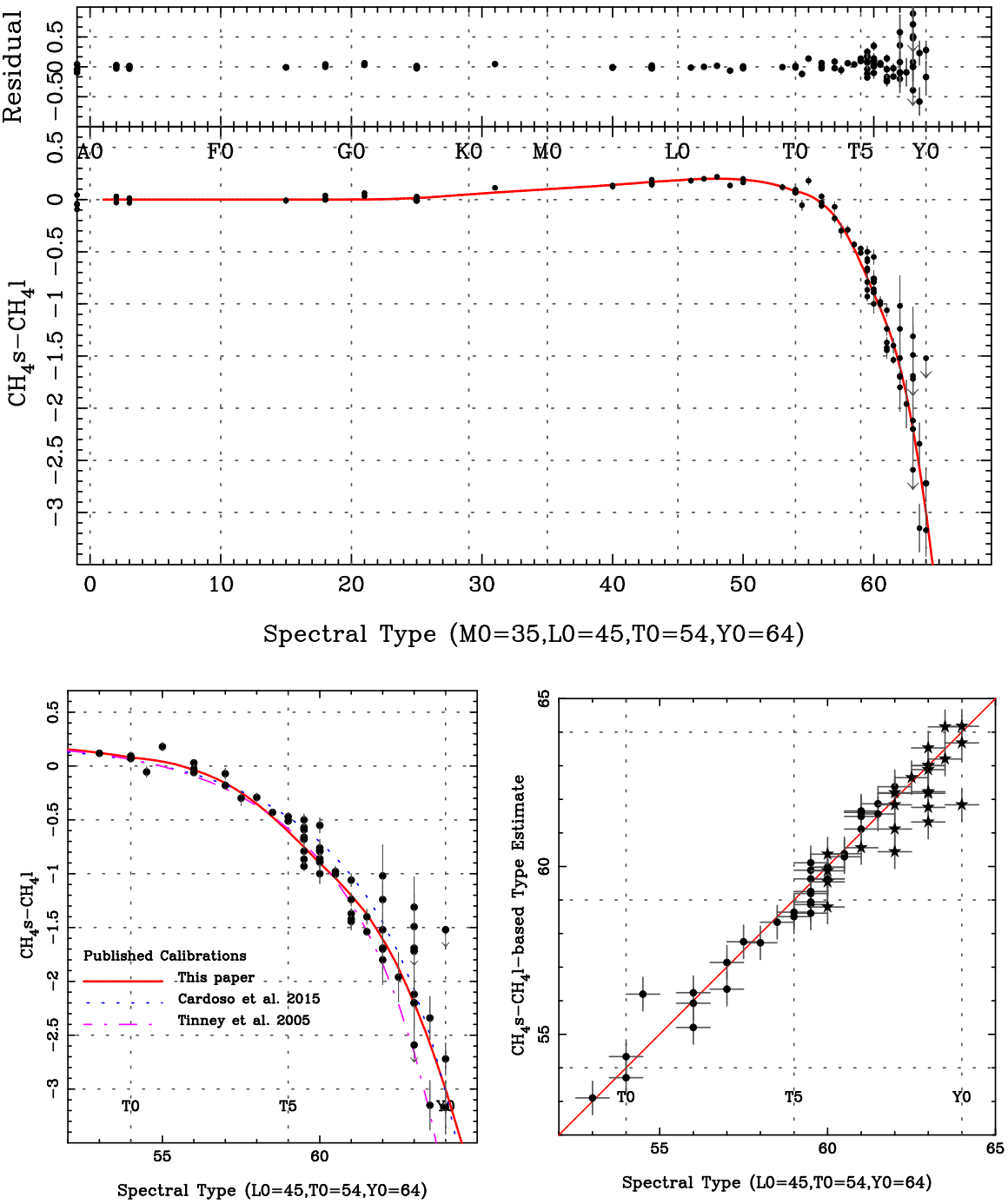

Figure 4. *Upper panel* – Methane-sensitive CH_4s-CH_4l as a function of A-Y spectral type. The uncertainties plotted are the combination of photon-counting uncertainties, aperture correction uncertainties and photometric calibration uncertainties. Typical uncertainties on spectral types (not plotted) are ±0.5. The plotted parametrisation is a spline constrained at the locations in Table 8. Root-mean-square (rms) scatter about the parametrisation is 0.18 mag for the whole range, 0.06 mag for L0-T2 dwarfs and 0.12 mag for T3-T8 dwarfs, and 0.45 mag for T9-Y0 dwarfs. The corresponding spectral type scatters are 0.6 sub-type for L0-T2 dwarfs and 0.43 sub-type for T3-T8 dwarfs, and 0.6 sub-type for T9-Y0 dwarfs. *Lower right panel* – Upper panel zoomed in on the T and Y dwarf region, with the previously published calibration relations due to Tinney et al. (2005) and Cardoso et al. (2016) also shown. *Lower left panel* – Comparison of the predicted spectral types from this CH_4s-CH_4l relation with observed spectral types (solid circles - Tinney et al. (2005); solid stars – this paper).

the measured bandpasses (in order of decreasing width): HST filter F125W 1.10-1.40 μm for Schneider et al.; J3=1.21-1.37 μm for Faherty et al.; and HST filter F127M 1.24-1.31 μm for Luhman & Esplin. Faherty et al. measured J3=$24.8^{+0.5}_{-0.35}$, following which Schneider et al. reported F125W=26.41±0.27 and Luhman & Esplin a mean value of F127M=24.45±0.1 from 3 observations (all Vega-magnitudes). When one considers the different bandpasses, these magnitude differences make sense. F125W includes substantial water vapour and methane absorption in its wider band-pass than J3. So the F125W Vega-magnitude should be fainter than J3. In turn J3 includes slightly more molecular absorption than F127M, which selects out a Y-dwarf flux peak. The significant "discrepancy" that Schenider et al. note with the result of Faherty et al. is not in the observed detections in these three bands, but rather in J magnitudes derived after conversion from the measured bandpass. For the Faherty et al. J3 detection, this was done using an empirical colour correction based on (hotter) T and Y dwarfs, which is clearly not appropriate for this very cool object.

We have J2 and J3 photometry for a smaller range of spectral types than we have CH_4s and CH_4l – i.e. only spanning T5.5 to Y1. These data are plotted in the upper panel of Fig. 5. Recalling that our J3−J2 system is defined so that objects in the A-G spectral type range will have J3−J2=0, the observation of a significantly negative J3−J2 colour does clearly distinguish T and Y dwarfs from much hotter field stars. The simple linear fit to these data in the figure is parametrised as a function of a modified numeric spectral type n', such that $n' = n - 60$ (making $n' = 4$ equivalent to a Y0), as

$$\mathrm{J3} - \mathrm{J2} = -1.12 - 0.097\,n',$$

with rms scatter of 0.19 mag.

Unfortunately, it would appear that the ability to observe fainter targets in J3/J2 comes at the penalty of obtaining less information on the spectral types of those objects. The J3−J2 colour appears to "saturate" at J3−J2 ≈ −1.5 for late-T and Y dwarfs – a range of spectral types over which CH_4s–CH_4l continues to become more-and-more negative for later objects. Moreover Y dwarfs are only ∼0.5 magnitudes more negative in J3−J2 than mid-T dwarfs, and the scatter about any trend is substantial at ±0.18 mag. The equivalent numbers for CH_4s−CH_4l are ∼ 3 mag and ±0.45 mag. This means that while J3−J2 can unequivocally identify a very cool brown dwarf's near-infrared counterpart (given the prior information that a cool dwarf is expected at that position from a large survey like *WISE*), it cannot provide a very good estimate of *how* cool that brown dwarf is.

6.3. *J3− W2 versus Spectral Type*

However, all is not lost, because the ability of J3−J2 to unequivocally associate a near-infrared source with a *WISE* thermal-infrared one, means that its J3−W2 colour is therefore determined. J3−W2 is primarily sensitive to effective temperature by sampling stellar flux in gaps between the strongest molecular absorptions over a long wavelength baseline, as has already been shown for J−$W2$ by Cushing et al. (2011) and Kirkpatrick et al. (2012) – as distinct to the methane colours CH_4s–CH_4l and J3−J2 which are sensitive to effective temperature by measuring the strength a specific molecular absorption.

As the lower panel of Fig. 5 demonstrates, J3−W2 shows a pronounced trend with spectral type, and while the scatter about a quadratic fit to these data is substantial (we again parametrise this fit as a function of a modified numeric spectral type n' such that $n' = n - 60$

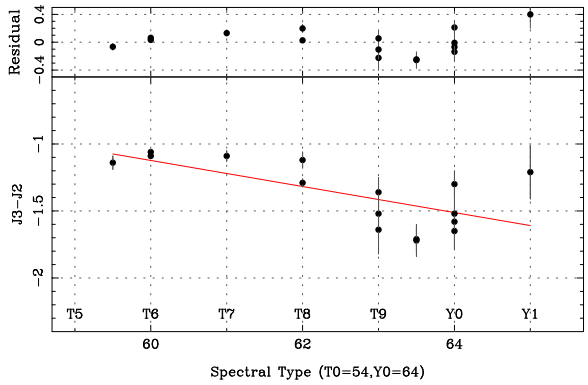

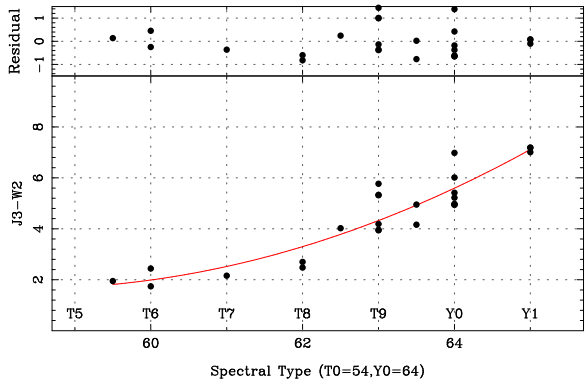

Figure 5. *Upper panel* – Methane-sensitive J3−J2 as a function of T5.5-Y1 spectral type. The uncertainties plotted are the combination of photon-counting uncertainties, aperture correction uncertainties and photometric calibration uncertainties. Typical uncertainties on spectral types (not plotted) are ±0.5. The plotted linear fit is described in §6.2, and has rms 0.19 mag.

Lower panel – Temperature-sensitive J3−W2 as a function of T5.5-Y1 spectral type. Along with the objects in Table 4, we also show nine objects with J3 and W2 (but without J2) from Tinney et al. (2014). The uncertainties are as for the upper panel. The plotted parametrisation is a quadratic fit described in §6.3, with rms 0.65 mag.

meaning a Y0 dwarf has $n' = 4$)

$$\mathrm{J3} - \mathrm{W2} = 1.99 + 0.4090\, n' + 0.12313\, n'^2,$$

with rms=0.65 mag, it also spans a large range in J3−W2 of over 5.5 mag. This means that its discriminating power for assigning an estimated spectral type is similar to that of the CH_4s−CH_4l colour over this spectral type range. For convenience we show the value of this parametrisation as a function of spectral type in Table 9.

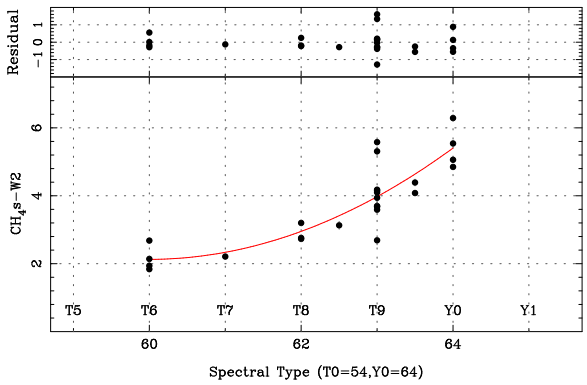

Figure 6. Temperature-sensitive CH_4s−W2 as a function of T6-Y0 spectral type. Uncertainties are as for Figure 5. The plotted parametrisation is a quadratic fit described in §6.3, with rms 0.60 mag.

In Figure 6 we show the equivalent plot to the lower panel of Figure 5, but based on CH_4s–W2 colour instead of J3–W2. CH_4s–W2 colour has a similar "lever arm" on spectral type as J3–J2, spanning a smaller range in colours (3.5 mag.), with a slightly smaller rms of 0.60 mag. The equivalent polynomial fit is

$$CH_4\mathrm{s} - \mathrm{W2} = 2.13 + 0.00519\, n' + 0.20357\, n'^2.$$

It is important to note, however, that observation of a candidate *WISE* counterpart in J3 or CH_4s (or indeed J or H) alone *is not sufficient to make a cool brown dwarf identification*. J2 or CH_4l is essential to obtain a clear identification of methane absorption. Without that identification, the association of a chance (usually faint) background source will invariably result in a large, *but completely spurious*, J3−W2 or CH_4s–W2 colour. Both J3 and J2 methane sensitive bands are to identify a near-

infrared, methane-absorbing counterpart, following which J3−W2 or CH_4s–W2 can provide an estimate of how cool that object is.

6.4. *New Y Dwarfs*

W0302-5817 is one of two new Y dwarfs presented for the first time in this paper. Its spectrum (obtained in 2017 Jan) is of low signal-to-noise but does clearly indicate a Y0 spectral type. This allows us to make a distance estimate using both its J3 and W2 photometry. The mean correction between J_{MKO} and J3 for cool dwarfs (J_{MKO}−J3 = 0.20±0.03) and the median J_{MKO} absolute magnitude for Y0 dwarfs (Tinney et al. 2014, M_J=20.32±1.25, giving a median M_{J3}=20.12±1.25), gives a distance for W0302-5817 lying in the range 24-7.5pc. A better estimate can be obtained using W2 (the median absolute magnitude for a Y0 has much lower scatter – M_{W2} = 14.65±0.35), which predicts d=17.5±3.5 pc. This places W0302 on the outer edge of the 20 pc sample of nearby brown dwarfs.

W1141-3326 is the second new Y dwarf presented here. As noted earlier, despite being observed with CH_4s,CH_4l filters in mid-2012, it took some time to obtain spectra for this object, because confusion with background sources meant its CH_4s–CH_4l colour was that of a mid-T dwarf, and so it was not made a high priority (see Fig. 2). A high quality spectrum was eventually obtained in 2014 March, and it is an excellent match to the template Y0 spectrum. W1141-3326's W2 photometry indicates a likely distance in the range 11.4-8.0 pc. This is a distance fully consistent with the preliminary trigonometric distance presented in Tinney et al. (2014) of 9.5±0.4 pc.

Both W1141-3326 and W0302-5817 are targets of our on-going parallax program with FourStar on the Magellan Baade telescope (Tinney et al. 2014).

6.5. *Comparison with Extant Spectroscopy*

Table 10 compares previously published spectral types for objects where we present new spectra, as well as objects where we identify the object as a T dwarf but do not have spectroscopy. For W1433−0837 and W1448−2534 we obtain the same spectral types from completely independent spectra and typing processes, while for W2212−6931 we obtain a type different by only 0.5 sub-types, which we consider to be consistent – especially as examination of Fig. 8 in Schneider et al. (2015) suggests that W2212−6931 has the narrowest 1.3 μm peak of of all the T9 objects shown, and so is possibly the closest to T9.5 in that group on their classification system.

We have not been able to obtain a spectrum for W0404−6420, and the T9 classification of Schneider et al. (2015) is 2 sub-types later from that estimated by our CH_4s–CH_4l photometry. This is 3-4 times larger larger than the 0.43-0.6 sub-type scatters observed in our calibration (Fig. 4), which reinforces our view that while a methane absorption detection is robust for identifying a cool brown dwarf, and the colour provides an estimate of the spectral type, spectroscopy remains the "gold standard' for a firm classification.

7. CONCLUSION

Our results show that – despite using a modest 4m-class telescope like the AAT on targets at J∼20 – methane imaging is an effective technique for refining cool dwarf candidate lists arising from an external survey. These are magnitudes at which near-infrared spectroscopy on a 4m telescope would be almost impossible, or at least prohibitively expensive. Methane imaging observations make both identifications and

Table 9. J3−W2, CH_4s−W2 versus Spectral Type

SpT	J3−W2	J3−W2	SpT	J3−W2	J3−W2	SpT	J3−W2	J3−W2
T5	1.70	···	T8	3.30	2.95	Y0	5.60	5.41
T6	1.98	2.13	T9	4.32	3.97	Y0.5	6.33	···
T7	2.52	2.34	T9.5	4.93	4.64	Y1	7.11	···

Table 10. Comparison with Extant Spectroscopy

Object	CH_4s−CH_4l "Type"	SpT (this paper)	SpT (other)	Reference
W0404−6420	T7.1±0.5	···	T9	Schneider et al. 2015
W1055−1652	>T8.2	T9±0.5	T9.5	Martin et al. 2018
W1433−0837	···	T8±0.5	T8	Lodieu et al. 2012
W1448−2534	T6.4±0.5	T8±0.5	T8	Thompson et al. 2013
W2212−6931	Y0.2±0.5	T9.5±0.5	T9	Schneider et al. 2015

first-estimates of the spectral type in a single observation – without having to obtain spectra for the multiple candidate targets that can usually be found in the substantial positional error boxes that arise from a survey like *WISE* .

Cool brown dwarfs from a large area, but shallow, survey like *WISE* will reside quite close to the Sun, and almost invariably have significant proper motions. As such the position error box to search in a follow-up program grows with time. Indeed it has been our experience, that substantial proper motions (i.e. $> 0.2''$/year) are so ubiquitous for *WISE* brown dwarfs, that once follow-up extended more than a few years beyond the baseline of the *WISE* mission, any objects which *do* positionally match with the *WISE* source to better than about half an arcsecond, are invariably found to *not* be cool brown dwarfs, but rather background sources.

We have shown that methane imaging observations – either in the H-band using CH_4s & CH_4l filters or in the J-band using J2 & J3 filters – can rapidly and efficiently identify *and preliminarily classify* cool brown dwarf candidates that arise from large, all-sky surveys like *WISE*.

We have presented data identifying 21 new T dwarfs and 2 new Y dwarfs from the *WISE* All-Sky Survey using methane imaging (in addition to the Y dwarf W1639 previously published by Tinney et al. 2012). In many cases these identifications were made for objects using a 4m-class telescope (the AAT) for objects at J$\gtrsim$20 – magnitudes at which near-infrared spectroscopy on such a telescope would be either impossible or prohibitively expensive.

We present a further 5 late T dwarfs (W0309-5016, W0628-8057, W2017-3421, W2211-4758) and 3 early T dwarfs (W0042-5840, W2302-7134, W2354-8140) with methane identifications, for which typing spectroscopy is required.

CGT gratefully acknowledges the support of ARC Australian Professorial Fellowship grant DP0774000 and ARC Discovery Outstanding Researcher Award DP130102695. We are grate-

ful for the extraordinary support we have received from the AAT's technical staff – K. Fiegert, Y. Kondrat, S. Lee, R. Paterson, and D. Stafford. Australian access to the Magellan Telescopes was supported through the National Collaborative Research Infrastructure Strategy of the Australian Federal Government. Travel support for Magellan and AAT observing was provided by the Australian Astronomical Observatory.

This publication makes use of data products from the Wide-field Infrared Survey Explorer, which is a joint project of the University of California, Los Angeles, and the Jet Propulsion Laboratory/California Institute of Technology, funded by the National Aeronautics and Space Administration. This publication also makes use of data products from 2MASS, which is a joint project of the University of Massachusetts and the Infrared Processing and Analysis Center/California Institute of Technology, funded by the National Aeronautics and Space Administration and the National Science Foundation. This research has made extensive use of the NASA/IPAC Infrared Science Archive (IRSA), which is operated by the Jet Propulsion Laboratory, California Institute of Technology, under contract with the National Aeronautics and Space Administration. This research has also benefitted from the M, L, and T dwarf compendium housed at DwarfArchives.org, whose server was funded by a NASA Small Research Grant, administered by the American Astronomical Society.

Facilities: AAT (IRIS2), Magellan:Baade (FourStar, FIRE), Keck::II (NIRSPEC), IRTF (SpeX), WISE, CTIO:2MASS

Software: Figaro, FIREHOSE (http://www.mit.edu/p Spextool (Cushing et al. 2004), ORACDR (http://www.jach.hawaii.edu/JACpublic/UKIRT/softwa

REFERENCES

Bertin, E. & Arnouts, S., 1996, A&AS, 117, 393
Burgasser, A. J., Geballe, T. R., Leggett, S. K., Kirkpatrick, J. D., & Golimowski, D. A. 2006, ApJ, 637, 106
Cardoso, C. V. et al., 2015, MNRAS, 450, 2486
Cavanagh, B., Jenness, T., Economou, F. & Currie, M. J., 2008, AN, 329, 295
Cushing, M. C., Vacca, W. D., & Rayner, J. T. 2004, PASP, 116, 362
Cushing, M. C., Kirkpatrick, J. D., Gelino, C. R., et al. 2011, ApJ, 743, 50
Dupuy, Trent J., Liu, Michael C. and Leggett, S. K., 2015, ApJ, 803, 102
Horne, K. 1986, PASP, 98, 609
Faherty, J. K. and Beletsky, Y. and Burgasser, A. J. & Tinney, C. and Osip, D. J. and Filippazzo, J. C. & Simcoe, R. A., 2014, ApJ, 790, 90
Kirkpatrick, J. D., Cushing, M. C., Gelino, C. R., et al. 2011, ApJS, 197, 19
Kirkpatrick, J. D., Gelino, C. R., Cushing, M. C., , et al. 2012, ApJ, 753, 156
Kirkpatrick, J. D., Cushing, M. C., Gelino, C. R. et al. 2013, ApJ, 776, 128
Kirkpatrick, J. D., Schneider, A.C., Fajardo-Acosta, S., et al. 2014, ApJ, 783, 122
Kirkpatrick, J. D., Kellogg, K., Schneider, A.C., et al. 2016, ApJS, 224, 36
Lodieu, N., Burningham, B., Day-Jones, A., et al. 2012, A&A, 548, A53
Liu, Michael C., Dupuy, T. J.; Bowler, B. P.; Leggett, S. K.; Best, W. M. J, 2012, ApJ, 758, 57.
Lucas, P. W., Tinney, C. G., Burningham, B., et al. 2010, MNRAS, 408, L56
Luhman, K. L., Burgasser, A. J. and Bochanski, J. J., 2011, ApJ, 730, L9
Luhman, K. L., 2014, ApJ, 786, L18
Luhman, K. L. & Esplin, T. L., 2016, AJ, 152, 78
Mace, G. N., Cushing, M. C., Skrutskie, M., et al. 2013, ApJ, 726,30, 205, 6
Mainzer, A. K. & McLean, Ian S. 2003, ApJ, 597, 555

Mainzer, A., Bauer, J., Grav, T. et al. 2011, ApJ, 731, 53
Martin, E. C., et al. 2018, in prep.
McLean, I. S., Becklin, E. E., Bendiksen, O., et al. 1998, Proc. SPIE, 3354, 566
McLean, I. S., Graham, J. R., Becklin, E. E., et al. 2000, Proc. SPIE, 4008, 1048
McLean, I. S., McGovern, M. R., Burgasser, A. J., et al. 2003, ApJ, 596, 561
Nakajima, T., Oppenheimer, B. R., Kulkarni, S. R., Golimowski, D. A., Matthews, K., Durrance, S. T., 1995, Nature, 378, 463
Oppenheimer, B. R., Kulkarni, S. R., Matthews, K., Nakajima, T., 1995, Science, 270, 1478
Persson, S. E., Murphy, D. C., Smee, S., et al. 2013, PASP, 125, 654
Pinfield, D. J., Gromadzki, M., Leggett, S. K. et al. 2014, MNRAS, 444, 1931
Rayner, J. T., Toomey, D. W., Onaka, P. M., Denault, A. J., Stahlberger, W. E., Vacca, W. D., Cushing, M. C., & Wang, S. 2003, PASP, 115, 362
Rosenthal, E. D., Gurwell, M. A., Ho, Paul T. P., 1996, Nature, 384, 243
Schneider, A.C., Cushing, M.C., Kirkpatrick, J.D., et al. 2015, ApJ, 817, 112
Schneider, A.C., Greco, J., Cushing, M.C., et al. 2016, ApJ, 804, 92
Schneider, A.C., Cushing, M.C., Kirkpatrick, J.D., Gelino, C. R., 2016, ApJ, 823, L35
Skrutskie, M. F., Cutri, R. M., Stiening, R., et al. 2006, AJ, 131, 1163
Simcoe, R. A., et al. 2008, Proc. SPIE, 7014
Simcoe, R. A., et al. 2010, Proc. SPIE, 7735
Thompson, M. A., Kirkpatrick, J. D., Mace, G. N. et al., 2013, PASP, 125, 809
Tinney, C. G., Burgasser, A. J., Kirkpatrick, J. D., & McElwain, M. W. 2005, AJ, 130, 2326
Tinney, C. G. et al. 2012, ApJ, 759, 60
Tinney, C. G., Faherty, J.K., Kirkpatrick, J.D., Cushing, M., Morley, C.V., Wright, E.L., 2014, ApJ, 796, 39
Tokunaga, A. T., Simons, D. A., & Vacca, W. D. 2002, PASP, 114, 180
Vacca, W. D., Cushing, M. C., & Rayner, J. T. 2003, PASP, 115, 389
Wright, E. L., et al. 2010, AJ, 140, 1868
Herbst, T. M., Thompson, D., Fockenbrock, R., Rix, H.-W., Beckwith, S. V. W., 1999, ApJL, 526, L17